Natural Resources Canada | Ressources naturelles Canada

GEOLOGICAL SURVEY OF CANADA
OPEN FILE 8811

# New core and downhole geophysical data sets from the Bells Corners Borehole Calibration Facility Ottawa, Ontario

H.L. Crow, K.D. Brewer, T.J. Cartwright,
S. Gaines, D. Heagle, A.J.-M. Pugin, H.A.J. Russell

2021

Canada


**GEOLOGICAL SURVEY OF CANADA**
**OPEN FILE 8811**

# New core and downhole geophysical data sets from the Bells Corners Borehole Calibration Facility, Ottawa, Ontario

**H.L. Crow[1], K.D. Brewer[1], T.J. Cartwright[1], S. Gaines[2], D. Heagle[3], A.J.-M. Pugin[1], H.A.J. Russell[1]**

[1]Geological Survey of Canada, 601 Booth Street, Ottawa, Ontario
[2]CanmetMINING, 1 Haanel Drive, Ottawa, Ontario
[3]CanmetENERGY, 1 Haanel Drive, Ottawa, Ontario

## 2021



Permanent link: https://doi.org/10.4095/328837

This publication is available for free download through GEOSCAN (https://geoscan.nrcan.gc.ca/).

**Recommended citation**
Crow, H.L., Brewer, K.D., Cartwright, T.J., Gaines, S., Heagle, D., Pugin, A.J.-M., and Russell H.A.J., 2021. New core and downhole geophysical data sets from the Bells Corners Borehole Calibration Facility, Ottawa, Ontario; Geological Survey of Canada, Open File 8811, 1 .zip file. https://doi.org/10.4095/328837

Publications in this series have not been edited; they are released as submitted by the author.

# Abstract

The Geological Survey of Canada's deep borehole test site at the Bells Corners Borehole Calibration Facility in Ottawa, Ontario, has been in use since the 1980's for the development and calibration of geophysical logging instrumentation. Cores from six deep boreholes (up to 300 m) are preserved and remain available for research purposes. In 2019, the facility underwent repairs to reopen deep boreholes, replace surface casings, and install atmospheric monitoring equipment. This report documents new laboratory core testing and downhole geophysical logs collected in borehole BC81-2, the most frequently logged of the boreholes at the facility. Core data sets include physical, mechanical, and hydraulic properties, nuclear magnetic resonance, and complex resistivity measurements. The downhole log suite includes televiewer imagery (optical and acoustic), total gamma, full waveform sonic, and fluid measurements (high resolution temperature, conductivity, and flow meter measurements). Digital data are provided in appendices. These data sets support ongoing collaborations at the Facility across a variety of disciplines for geological exploration, geoengineering, and hydrogeological research.

# Contents

# 1.0 Introduction

In the late 1970's and early 1980's, the Geological Survey of Canada (GSC) established a test site in Ottawa, Ontario, for the development and calibration of borehole geophysical instruments and techniques. The facility is located near the Canada Centre for Mineral and Energy Technology (CANMET) research laboratories in Bells Corners (Figure 1). The Bells Corners Borehole Calibration Facility (Bells Corners) is composed of two separate outdoor sites: the first is a series of nine concrete columns for downhole gamma ray spectrometer calibration, and the second is a series of six deep bedrock calibration boreholes (73m – 300m) with preserved cores. The boreholes intersect various bedrock types (carbonate, sandstone, igneous) and structures, with a wide variety of physical and mineralogical properties.

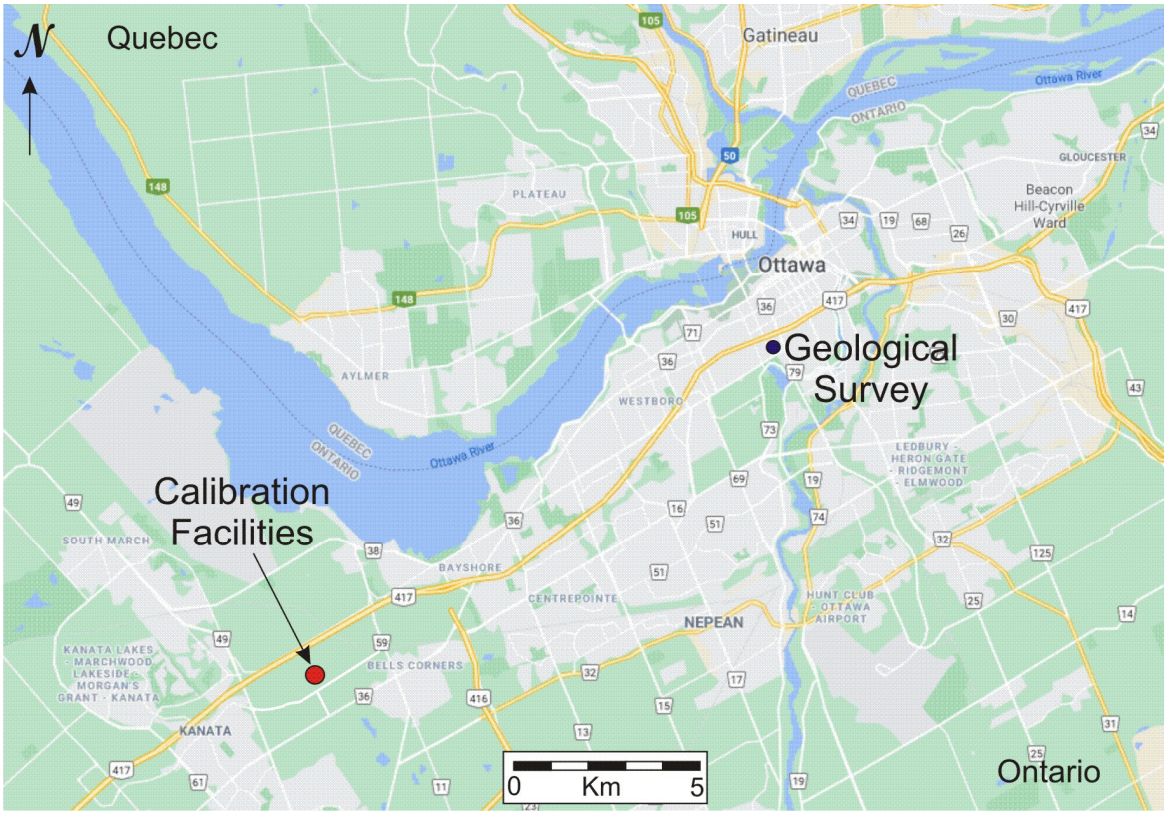


Figure 1. Location of GSC calibration facilities (map background: Google, n.d.).

Historically, the facility played a significant role in the advancement of Canadian geophysical logging instrumentation in the 1980's and 90's at a time when logging tools and techniques were being developed and deployed for mineral exploration (Killeen et al., 1984; Killeen, 1986; Schock et al., 1996). The site provided a facility where academia and industry could test and calibrate their instruments against a data set of documented physical properties (Bernius, 1996; Mwenifumbo et al., 2005). Today, instrument development and calibration remain at the core of the facility's importance to industry, government, and academia, and the facility continues to serve clients in the extractive, geotechnical, and environmental sectors.

Interest in the site over the past few years is becoming more multi-disciplinary. The need for monitored deep borehole sites in Canada is increasingly important for long-term research into groundwater flow through fractured bedrock, and surface to groundwater interaction (e.g. the growing international network of critical zone observatories). In response to an increasing interest in access to Bells Corners and digital calibration data sets, casings at the deep boreholes were repaired in 2019 and the GSC collected a new series of geophysical logs with modern tools to complement the existing suite of geophysical data. New, high-resolution imagery with optical and acoustic televiewers provide context for studying hydrogeological conditions at the site, alongside repeat groundwater temperature, conductivity and flow measurements. Core testing was also carried out in 2019 and 2020 to provide an expanded set of physical, mechanical, and hydrological calibration data in the various bedrock types intersected by the boreholes.

This report describes the new core and downhole calibration data sets acquired in borehole BC81-2, with digital data included in appendices. The use of trade or product names throughout this report is for descriptive purposes only and does not represent endorsement by Natural Resources Canada. These data sets are provided to support ongoing collaborations at Bells Corners across a variety of disciplines for geological exploration, geoengineering, and hydrogeological research.

## 2.0 Outdoor calibration facilities

The Bells Corners Borehole Calibration Facility is composed of two separate outdoor sites at the CANMET complex in Ottawa (Figure 2). The first is a series of nine, above-ground concrete test columns containing natural variations in potassium (K), uranium (U), and thorium (Th) for the calibration of spectral gamma-ray logging tools. The columns were built in 1977 by the GSC in response to the International Atomic Energy Agency (IAEA, 1976) recommendations on the calibration of radiometric exploration equipment (Killeen, 1978; Killeen and Conway, 1978). More information about the radioelement concentrations for each column can be found in Mwenifumbo et al. (2005). The second facility consists of six deep bedrock boreholes ranging in depth from 73m to 300m. The test site was established in the early 1980's by the GSC for the development and calibration of geophysical instruments (Killeen, 1986), and is the focus of this report.

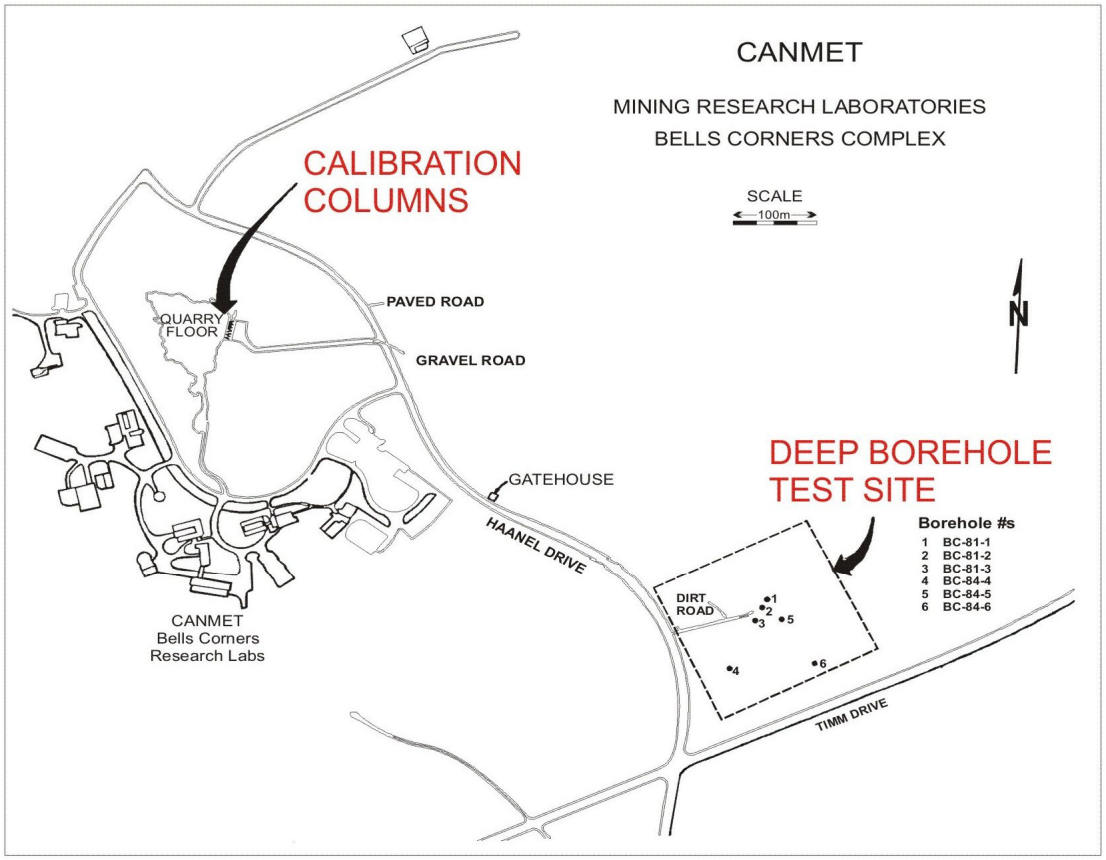


Figure 2. Map showing the location of the calibration facilities at the Bells Corners CANMET complex (adapted from Mwenifumbo et al., 2005).

### 2.1 Deep bedrock borehole test site

Six vertical holes were drilled by Longyear Canada Inc. in 1981 and 1984 (Bernius, 1981; Killeen et al., 1984). The boreholes were laid out in a triangular configuration spaced 10m, 20m, 30m, 70m, and 100m apart for cross-hole testing (Figure 3). Boreholes 1, 2, 3, and 5 were collared on top of a pad several metres in thickness, while boreholes 4 and 6 were drilled directly into bedrock. Recovery of NQ cores (47mm diameter) was high, and the cores continue to be stored in Ottawa as part of the GSC's Earth Materials Collections.

A compilation of downhole geophysical logs collected in the 80's and 90's is provided by Bernius (1996). Log types include nuclear (passive spectral gamma, active gamma-gamma density, neutron), electrical (induced polarization, resistivity, self potential), induction (magnetic susceptibility, conductivity), fluid logs (temperature, resistivity), sonic velocity, and borehole diameter (1- and 3-arm caliper). Of the six boreholes, the best documented and most frequently logged is BC81-2 as it contains all the geologic features found in the other holes and is the most accessible near the entrance to the site. As a result, BC81-2 is the focus of the new core and downhole calibration data sets published in this study, but updated information about the status of all the boreholes is provided below.

After nearly 40 years in use, borehole repairs were undertaken in 2019. Frost heave, settlement, and weathering had affected the integrity of metal surface casings. In boreholes 2, 3, 4, 5, and 6, the metal surface casings were replaced and reset solidly into rock (Figure 4a). Borehole 3 was enlarged from NQ to HQ to allow for larger diameter tools and deployments. In boreholes 4, 5, and 6, near-surface, vertical fractures created unsuitable conditions for lowering instruments into deeper parts of the wells so PVC screens (73mm ID) were used to case through shallow fracture zones - allowing for safe movement of logging tools while maintaining natural groundwater flow into the wells. Repairs were not undertaken in borehole 1 due to unstable conditions in the weathered zone at the top of the Precambrian bedrock; the sedimentary sequence remains accessible, but the borehole is not available for logging below 64m. Details of the borehole locations, depths, and open hole diameters can be found in Table 1, with details of the new casing installations in Table 2.

Atmospheric monitoring was also initiated at the site. Water level loggers were deployed in November 2018 in boreholes 1, 4, and 6 with a barometric sensor in borehole 1. The loggers record fluid temperature and pressure variation at a rate of 1 reading/hour. A small rain gauge and air temperature data logger were also installed in May 2019 between boreholes 4 and 6 (Figure 4b).

Table 1. Well co-ordinates and elevations based on differential GPS measurements recorded between 2019 and 2021. The horizontal datum is NAD83 and the vertical datum for the elevations (orthometric height) is CGVD28(HTv2.0). Drilling depths are as reported on core logging records from the 1980's. Depth Open based on camera inspections in 2019. bgs=below ground surface.

| Name | Lat | Long | Elevation (Top of Casing) (m) | Open hole diameter (mm) | Drilling Depth (m bgs) | Depth Open (m bgs) | Casing Stick-up (m) |
|---|---|---|---|---|---|---|---|
| BC81-1 | 45.318754 | -75.861179 | 115.45 ± 0.04 | 76 (NQ) | 299.20 | 64 | 0.23 |
| BC81-2 | 45.318670 | -75.861230 | 115.74 ± 0.04 | 76 (NQ) | 120.12 | 115 | 0.87 |
| BC81-3 | 45.318502 | -75.861336 | 115.30 ± 0.05 | 96 (HQ) | 119.50 | 73 | 0.54 |
| BC84-4 | 45.317933 | -75.861694 | 114.77 ± 0.03 | 76 (NQ) | 300.25 | 300 | 0.85 |
| BC84-5 | 45.318536 | -75.860965 | 114.71 ± 0.04 | 76 (NQ) | 248.97 | 249 | 0.84 |
| BC84-6 | 45.318020 | -75.860453 | 112.67 ± 0.03 | 76 (NQ) | 298.74 | 290 | 0.53 |

Table 2. Casing intervals and completion details. Depths reported relative to top of casing. Hole diameter in intervals containing PVC is 98.4mm (3-7/8”). OD of PVC casing is 88.9mm (3.5”). ID of PVC casing is 73.0mm (2-7/8”). At the time of publication, BC84-6 was awaiting logging.

| Name | Year of repair | Metal casing interval (m) | Solid PVC interval (m) | Slotted PVC interval (m) | Sand pack (m) | Bentonite seal (m) |
|---|---|---|---|---|---|---|
| BC81-1 | N/A | TOC – 5.31 (NQ) | N/A | N/A | N/A | N/A |
| BC81-2 | 2019 | TOC – 7.77 (PQ) | TOC – 7.89 | N/A | N/A | Surface – 7.89 |
| BC81-3 | 2019 | TOC – 6.10 (HQ) | N/A | N/A | N/A | N/A |
| BC84-4 | 2019 | TOC – 3.20 (PW) | TOC – 3.56 | 3.56 – 14.04 | 3.41 – 14.04 | Surface – 3.41 |
| BC84-5 | 2019 | TOC – 3.81 (PW) | TOC – 4.75 | 4.75 – 7.68 | 4.60 – 7.68 | Surface – 4.60 |
| BC84-6 | 2019 | - | - | - | - | - |

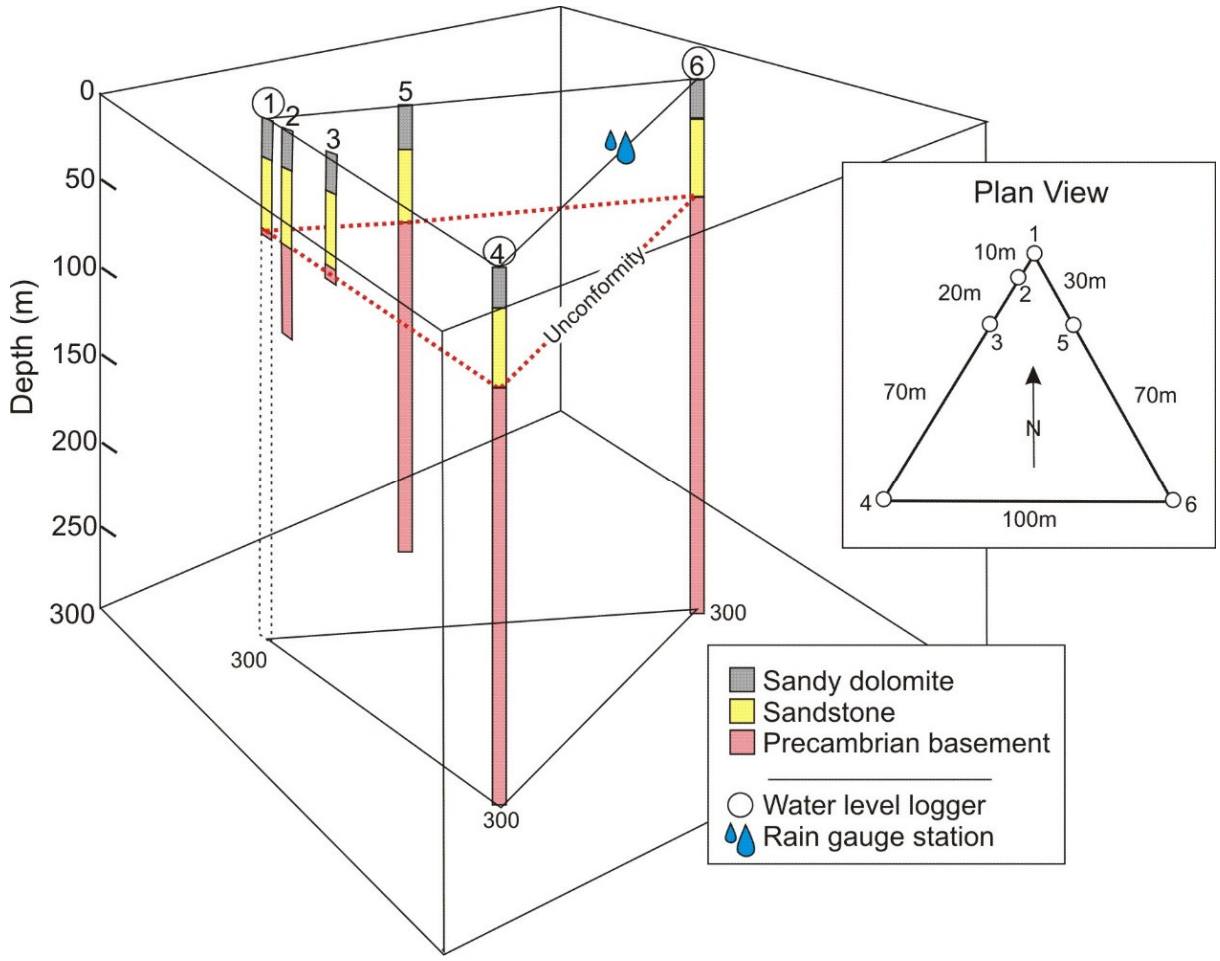


Figure 3. Positions and depths of boreholes in the Bells Corners deep borehole cluster (adapted from Mwenifumbo et al., 2005).


(a) (b)

Figure 4. Images from the Bells Corners deep borehole test site. (a) Borehole BC81-2. (b) Rain gauge and air temperature logger. Photographs by H.Crow. NRCan photos 2021-130 and 2021-131.

## 2.2 Geological context of the deep boreholes

The deep bedrock boreholes intersect Potsdam and lower Beekmantown Group sedimentary formations and terminate in highly variable Precambrian igneous and metasedimentary bedrock of the Grenville Province. The contact between the Precambrian basement and overlying sedimentary rock forms a significant regional unconformity spanning 0.5Ga (Di Prisco and Springer, 1991).

Precambrian bedrock, where outcropping in areas surrounding Ottawa, is Mesoproterozoic in age (0.9 – 1.6Ga) and is identified as part of the Grenville Supergroup (Hofmann, 1998; Davidson, 1998). Intensely deformed and metamorphosed, the strata of sedimentary and volcanic origins form part of the Central Metasedimentary Belt (CMB) in Ontario, southwest Quebec, and northern New York State (Wynne-Edwards, 1972; Easton, 1992; Davidson, 1998). The CMB in eastern Ontario contains stocks of potassic plutonic rocks (undeformed syenites and granites) dated to 1.1Ga (Corriveau et al., 1990).

The overlying Potsdam Group (Neoproterozoic to Lower Ordovician) regionally consists of alluvial conglomerate and feldspathic sandstone (Covey Hill Formation, absent in the Bells Corners boreholes), overlain by mostly marine, well-sorted, mature quartz arenites of the Keeseville (more commonly known as the Nepean) Formation (Salad Hersi and Dix, 2006; Sanford and Arnott, 2010; Lowe, 2016), which is present at the site. U-Pb dating indicate the sediments were derived from the underlying CMB and adjacent Precambrian highlands, transported into the area by fluvial processes (Chiarenzelli et al., 2010; Sanford and Arnott, 2010; Lowe et al., 2018). The nature of the upper contact between the Keeseville and overlying Theresa Formation has been a subject of some debate. Some see it as a conformable transition (Sanford and Arnott, 2010) while others have argued the transition contains a disconformity caused by a regional hiatus in sedimentation (Dix et al., 2004).

Overlying the Keeseville Formation, the boreholes intersect the Beekmantown Group (Lower to Middle Ordovician) that is composed of three formations deposited in a shallow marine, peritidal setting. The lowermost Theresa Formation is composed primarily of dolomitic sandstones (coarse-grained quartz arenite with fine-grained sandy quartzose dolostone interbeds) (Bernstein, 1992; Salad Hersi et al. 2003). The intermediate Beauharnois Formation is primarily dolostone with subordinate limestone, quartzose carbonate, and dolomitic and calcareous arenite (Bernstein, 1992). The uppermost Carillon Formation of the Beekmantown Group is not intersected at Bells Corners.

### Core descriptions and geophysical responses in BC81-2

The core from BC81-2 was originally logged by the GSC in 1981 and documented by Bernius (1981, 1996) and Killeen et al. (1984, 1986). The formation names originally used by the GSC are now updated with those adopted by the Ontario Geological Survey during regional remapping initiated in 2018. Characteristics of the rock are summarized from oldest to youngest, with observations added from recent core testing (described in Section 3).

Precambrian bedrock (core depths 64.30 – 120.12m)

The borehole terminates in gneissic bedrock (hornblende/biotite), containing intervals of fresh granite. Rock types include felsic granite, syenite, pegmatite, mafic chlorite-gneiss, and biotite-hornblende-scapolite gneiss, all having complex structural relationships that could not be traced between boreholes only tens of meters apart (Bernius, 1996). Geophysical logs indicate the gneissic zones generally produce elevated responses in the magnetic susceptibility, resistivity, and density, but lower levels of gamma response than in the granites. Core analyses indicate porosities <0.5%, and bulk densities ranging from 2.70 to 3.05g/cm$^3$.

A 17-m thick alteration zone extends upward to the Precambrian-Keeseville contact, consisting of alteration minerals (sericite, chlorite, epidote, hematite and calcite) along with quartz and plagioclase from the syenites and granites. Geophysical response in the alteration zone is marked by an increase in gamma log counts due to the potassium in the sericite and the feldspar (orthoclase). Electrical logs indicate reduced induced polarization (IP) and resistivity responses due to the weathered clay minerals, and magnetic susceptibility logs display relatively low responses as a result of alteration from magnetite to hematite. Core measurements in the weathered zone were difficult to collect as the clays swelled and crumbled during saturation, but porosity estimates range from 2.3% to 5.1%, and bulk densities from 2.50 – 2.62g/cm$^3$.

The top of the Precambrian is marked by a sharp unconformity. The surface is irregular and broken, containing a 30cm interval of highly weathered, friable pinkish-red clays and altered feldspars derived from syenite and granite, and greenish-grey saprolite derived from more mafic gneisses (Bernius 1996).

Keeseville (Nepean) Formation (core depths 20.45 – 64.30m)

The contact with the basement occurs at a 20cm thick quartz conglomerate with some brownish limonitic layers (Bernius, 1996). A 5.2m-long interval of white quartz sandstone overlies the conglomerate. Overlying this is a sandstone sequence characterized by alternating bioturbated and cross-bedded sandstone, both with variable amounts of hematite (visible iron staining), glauconite and limonite. There are 23 bioturbated layers identified, ranging in thickness from 5 to 83cm. Burrows are frequently seen in this interval. The upper 16m of the Keeseville Formation is characterized by massive, white quartz arenite with some dark laminae and irregular layers.

The geophysical logs indicate the lowermost 5m above the Precambrian contact is an interval of low gamma response. The gamma and electrical log responses in the overlying bioturbated layers are more varying. Correlations between gamma and electrical logs from the other boreholes indicates the lithologies in this interval are fairly continuous from hole to hole across the site (Bernius, 1996). The geophysical logs in the upper part of the Keeseville display relatively lower levels of total gamma counts, resistivity, and density. Core testing focused on intervals with variations in density. Within the upper quartz arenite, porosity ranged from 1.5% (2.57g/cm$^3$) to 12% (2.44g/cm$^3$) and can change over short (decimeter-scale) intervals. Samples selected within the bioturbated beds indicated porosity was relatively low 1.85 – 1.87% (2.58 - 2.60g/cm$^3$). Within a visibly more porous zone in the core in the lower interval of quartz arenite, porosities ranged from 8.4% to 9.4% (2.38 – 2.40g/cm$^3$).

Theresa and Beauharnois Formations (core depths 5.30 (top of core) – 20.45m)

The Theresa Formation is composed of interbedded sandy calcareous dolostone and calcareous sandstone. The base of the formation contains a distinct dark grey layer of uranium-bearing and chalcopyrite-rich pyrobitumen (Charbonneau et al., 1975; Bernius, 1996) also known as thucolite (see Hoekstra and Fuchs, 1960). The core transitions upward into a grey, fine to medium crystalline dolostone, containing a few very thin interbeds of fine grained quartz sandstone. Calcite-filled cavities are observed in core. The upper several metres of core are broken and fractured, with visible weathering along vertical fracture surfaces. The transitional nature of the Theresa Formation upward into the Beauharnois Formation leaves assigning the contact between the two open for re-examination. The local thickness of the Theresa Formation has been interpreted to be about 10m, suggesting that the upper few metres of core could be Beauharnois Fm.

The IP, resistivity, density and magnetic susceptibility logs show a general increase (and more variability) in the Theresa relative to the underlying Keeseville. Core testing over a 22cm-long sample indicates porosities range from 1.95 – 3.12% and bulk densities range from 2.56 – 2.61g/cm$^3$. At Bells Corners, the pyrobitumen layer creates a distinct marker horizon in the gamma logs with a sharp depth-discrete increase in uranium content. While this layer has been detected by gamma logs in other Ottawa GSC calibration boreholes (e.g. Lebreton and Observatory Crescent), it is not consistently observed region-wide, and therefore should not be considered a reliable regional geophysical marker horizon for the base of the Theresa.

Bedrock outcrops at the facility, with numerous road cuts and quarry walls available for examination within a few hundred metres of the boreholes (Figure 5).

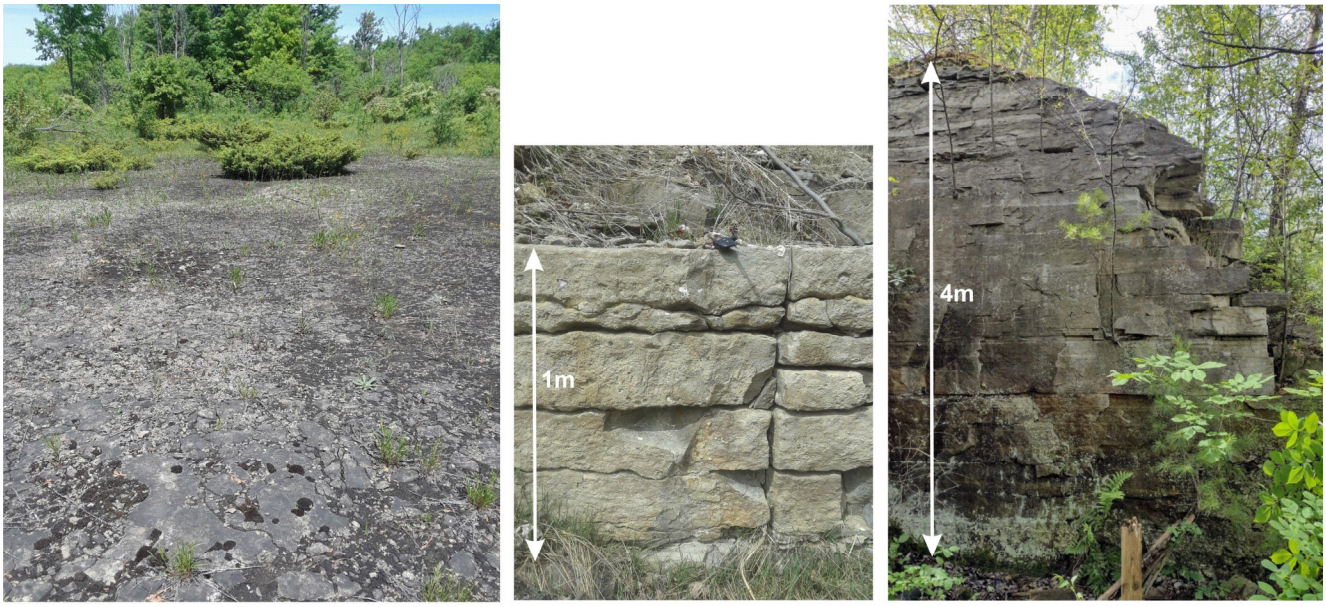


(a) (b) (c)

Figure 5. (a) Sandy dolomitic bedrock outcrops at the Bells Corners deep borehole test site. (b) Road cuts and (c) quarry walls near the test holes provide opportunities to examine shallow bedrock in section. Scales are approximate. Photographs by H.Crow. NRCan photos 2021-132, 2021-133, and 2021-134.

## 2.3 Hydrogeologic context of the deep boreholes

The Bells Corners test site is located on a topographic high (Figure 6) on the very edge of the Rideau Valley Conservation Area, within the Ottawa River West subwatershed, Stillwater catchment area. In the early 1980's, a hydrogeological study was undertaken in the Stony Swamp Conservation Area (in which the deep borehole test site is located) on behalf of the National Capital Commission (DelCan, 1983). An aspect of the study involved the identification of significant subsurface water flows and subsurface water system. The Precambrian bedrock was noted to have low transmissivity but could yield some water for domestic supply, whereas the Keeseville sandstone with near vertical joints is regionally known to be a productive aquifer. The overlying Theresa formation was described as being 'highly pervious' with vertical joints that can result in potentially productive wells. It was noted that the Hazeldean Fault zone, running south-west of the test site, has a significant impact on the movement of groundwater, appearing to form a barrier for the productive aquifers located north of the fault.

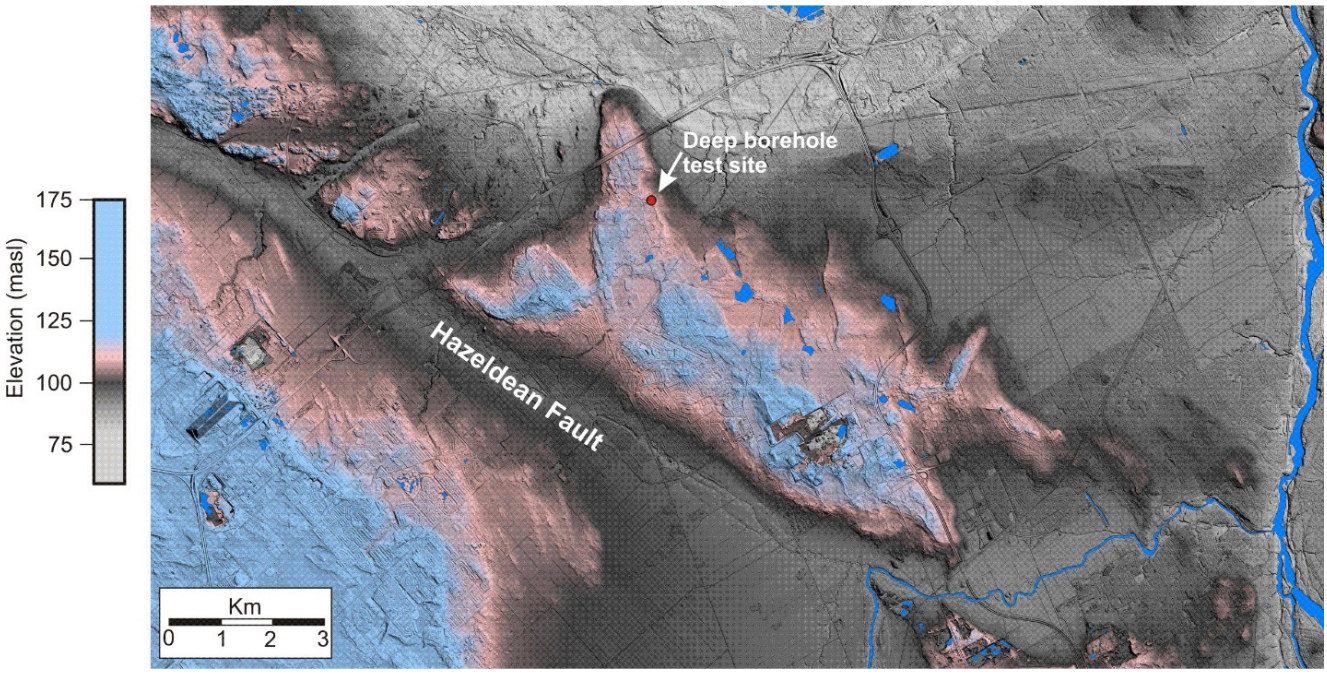


Figure 6. Shaded relief map of the calibration site and surrounding area derived from LiDAR DEM data, courtesy of the City of Ottawa.

At the site, steeply dipping fractures observed near the boreholes provide potential direct pathways for entry of surface water into the groundwater system (Figure 7). Monitoring of fluid and air temperatures, groundwater levels, and precipitation on site will provide new data sets to study the seasonal effects of groundwater temperatures and the connection between surface and groundwater. An initial round of monthly downhole temperature profiles in BC81-2 revealed seasonal changes in the near surface fluid temperatures (upper 15m) that lag behind air temperatures (Figure 8). These logs also provide useful data sets for shallow geothermal studies.

Flow meter measurements indicated that groundwater is flowing in both up and down directions in the cross-connecting, open boreholes. Up-flowing groundwater is entering the boreholes through fractures near the base of the Keeseville sandstone and exiting the borehole through fractures in the upper half of the formation. Down-flowing water is entering the boreholes from the same fracture at the base of the Keeseville and gradually being reassumed into deeper fractures within the Precambrian bedrock. The deepest measurement of downward flow at the site was recorded at 198m in borehole BC84-5. Ongoing characterization of the hydrogeological conditions is being conducted at the site.

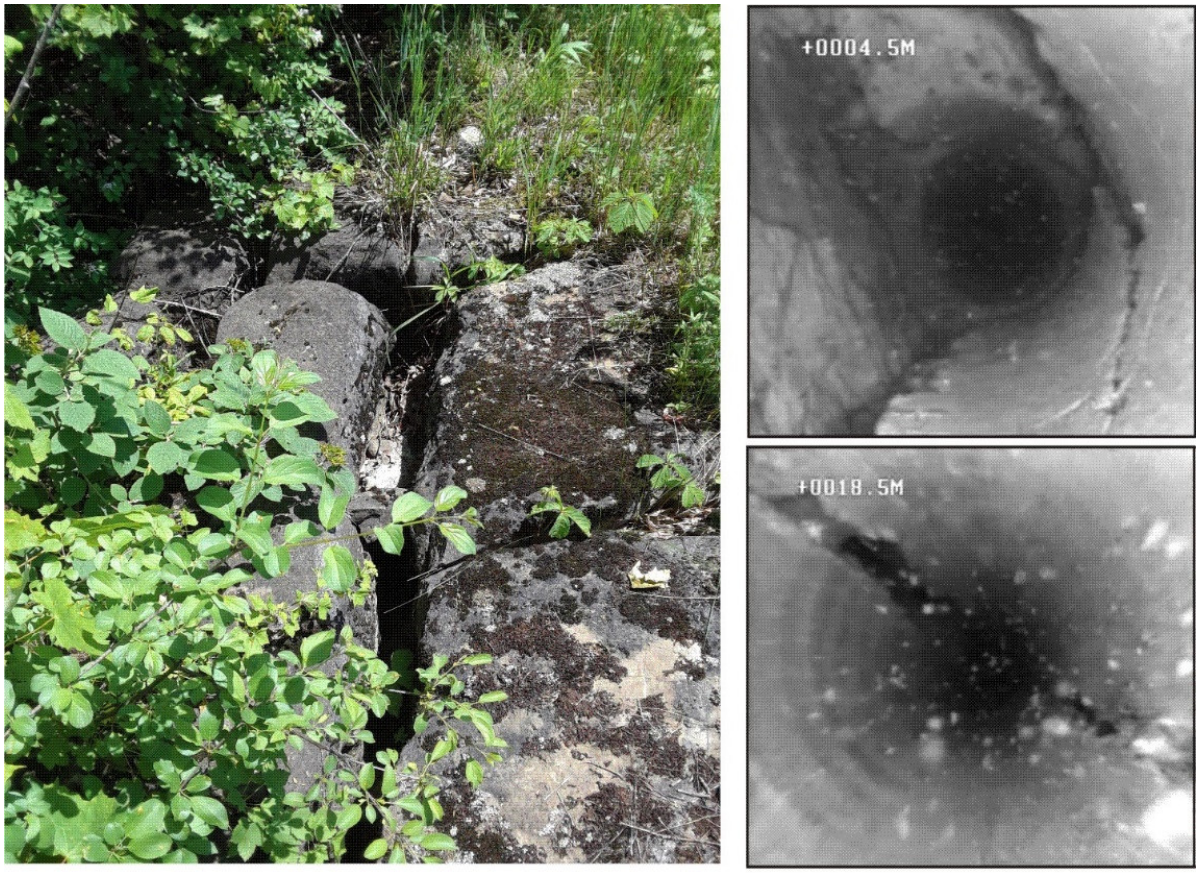


Figure 7. (a) Large vertical fracture adjacent to BC84-6. (b) Video camera images from BC84-6 show examples of vertical fractures persisting downhole at 4.5m (upper) and 18.5m (lower). Photograph by H.Crow. NRCan photo 2021-135.

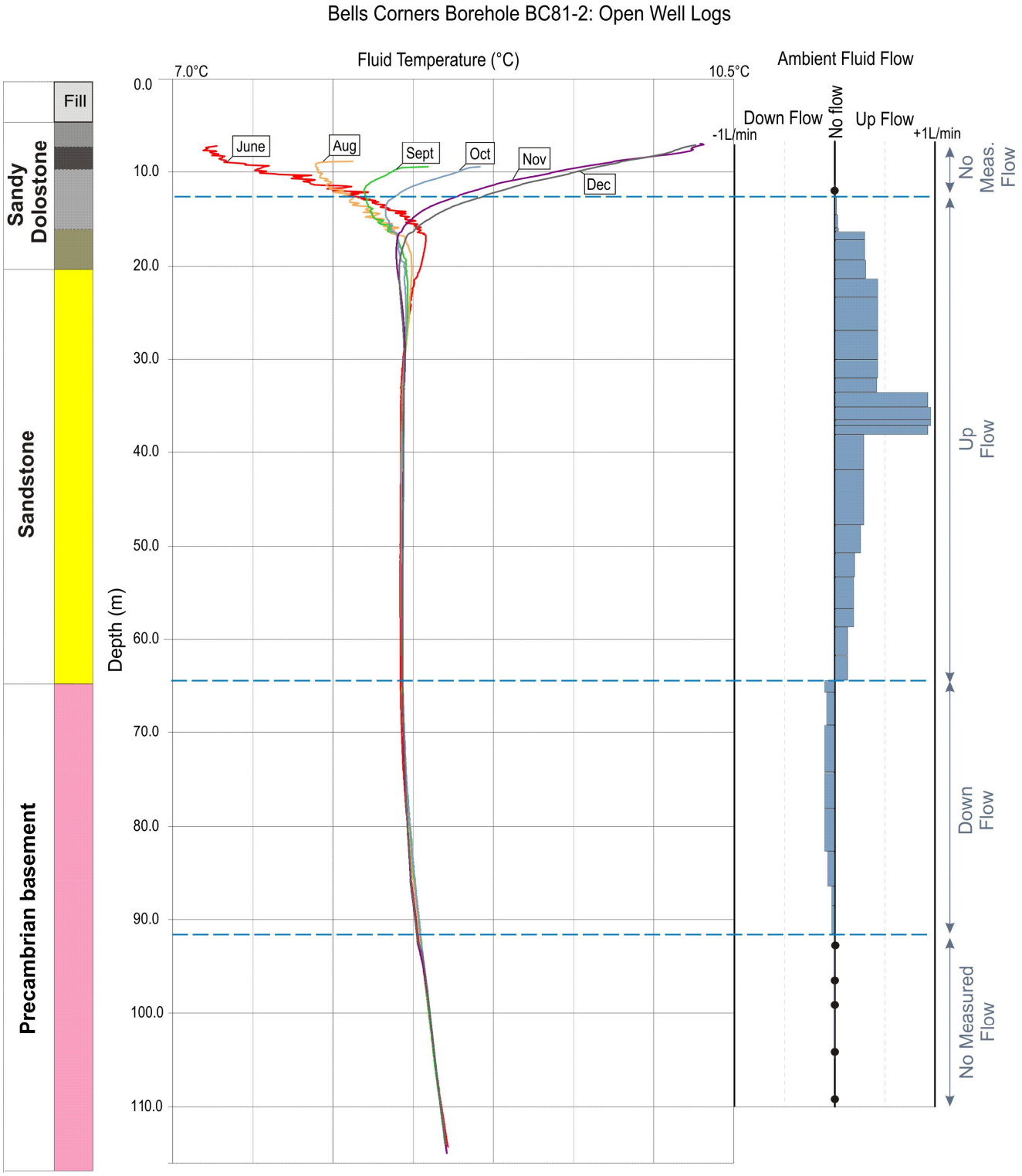


Figure 8. Monthly open hole temperature profiles in BC81-2 (June to December, 2019), shown alongside flow meter measurements collected in August 2019. The top reading of each log is the top of the water column at the time of logging.

# 3.0 Core measurements

A series of laboratory tests were carried out on cores from BC81-2 to provide a high-quality data set of rock properties for downhole instrument calibration. A distribution of intact samples along the core were selected in intervals where geophysical logs indicated rock properties were varying. Four laboratories conducted the testing:

- CanmetMINING's Rock Mechanics Laboratory in Ottawa measured physical, mechanical, and hydraulic properties of intact rock:
    - density, porosity, ultrasonic compressive (P) and shear (S) wave velocity,
    - uniaxial compression strength (UCS), triaxial compression strength (TCS), and Brazilian tensile strength (BTS) tests, and
    - constant head permeability to estimate intact rock permeability;
- CanmetENERGY Laboratories in Ottawa, and H2 Laboratories in Fredericton, New Brunswick, performed nuclear magnetic resonance (NMR) measurements to provide core porosity data; and
- TechnoImaging Inc. in Utah performed complex resistivity (CR) measurements as a function of frequency on six sandstone samples as part of their study examining the effect of increasing salinity on IP effects.

The depths of the various core tests are summarized in Table 3. The general condition of the core tested was very good, with exceptions noted in the Precambrian contact zone where cores could be crumbly.

Following the drilling in the 1980's, depth marks were scribed along the core at 10cm intervals. Differences have been noted between core depths and carefully calibrated wireline depths (from optical televiewer logs) in BC81-2 (see Section 4.3 for details on the analysis of depth offsets). All laboratory specimen intervals are reported as core depths (in metres below ground surface), and data tables 4 and 5 also contain a second depth column corrected to wireline depths (in metres below ground surface) to allow for comparison with geophysical logs.

Table 3. Summary of core tests from BC81-2.

| | Core depth from (m) | Core depth to (m) | Sample Name | Density | Porosity | Vp | Vs | UCS | TCS | BTS | Permeability | NMR | CR/IP |
|---|---|---|---|---|---|---|---|---|---|---|---|---|---|
| Dol. SST | 17.56 | 17.66 | BC81-2-1U | ✓ | ✓ | ✓ | ✓ | ✓ | | | | | |
| | 17.67 | 17.78 | BC81-2-2T | ✓ | ✓ | ✓ | ✓ | | ✓ | | ✓ | | |
| | 17.78 | 17.82 | BC81-2-1B | ✓ | ✓ | | | | | ✓ | | ✓ | ✓ |
| Sandstone | 29.58 | 29.69 | BC81-2-3U | ✓ | ✓ | ✓ | ✓ | ✓ | | | | | |
| | 29.70 | 29.80 | BC82-1-4T | ✓ | ✓ | ✓ | ✓ | | ✓ | | ✓ | | |
| | 29.82 | 29.85 | BC81-2-2B | ✓ | ✓ | | | | | ✓ | | ✓ | ✓ |
| | 29.86 | 29.90 | BC81-2-3B | ✓ | ✓ | | | | | ✓ | | ✓ | |
| | 34.66 | 34.69 | BC81-2-4B | ✓ | ✓ | | | | | ✓ | | ✓ | ✓ |
| | 34.70 | 34.74 | BC81-2-5B | ✓ | ✓ | | | | | ✓ | | ✓ | |
| | 34.75 | 34.78 | BC81-2-6B | ✓ | ✓ | | | | | ✓ | | ✓ | |
| | 37.42 | 37.45 | BC81-2-R1 | | | | | | | | | | ✓ |
| | 47.54 | 47.57 | BC81-2-7B | ✓ | ✓ | | | | | ✓ | | ✓ | ✓ |
| | 47.60 | 47.70 | BC81-2-5U | ✓ | ✓ | ✓ | ✓ | ✓ | | | | | |
| | 59.22 | 59.25 | BC81-2-8B | ✓ | ✓ | | | | | ✓ | | ✓ | ✓ |
| | 59.26 | 59.30 | BC81-2-9B | ✓ | ✓ | | | | | ✓ | | ✓ | |
| | 59.79 | 59.90 | BC81-2-6T | ✓ | ✓ | ✓ | ✓ | | ✓ | | ✓ | | |
| | 59.90 | 59.94 | BC81-2-10B | ✓ | ✓ | | | | | ✓ | | ✓ | |
| | 59.94 | 59.98 | BC81-2-11B | ✓ | ✓ | | | | | ✓ | | ✓ | |
| Weathered Precambrian | 66.71 | 66.81 | 66.71-U | | | ✓ | ✓ | ✓ | | | | | |
| | 66.84 | | 66.84-P | Weathered sample, crumbles | | | | | | | | | |
| | 66.99 | 67.09 | 66.99-U | | | ✓ | | ✓ | | | | | |
| | 67.20 | | 67.20-P | Weathered sample, crumbles | | | | | | | | | |
| | 67.20 | | 67.20-P2 | | | | | | | | | | |
| Precambrian | 70.94 | 71.04 | 70.94-U | | | ✓ | ✓ | ✓ | | | | | |
| | 71.09 | 71.19 | 71.09-T | ✓ | ✓ | ✓ | ✓ | | ✓ | | | | |
| | 71.20 | 71.30 | 71.20-U | | | ✓ | ✓ | ✓ | | | | | |
| | 75.87 | 75.97 | 75.87-U | | | ✓ | ✓ | ✓ | | | | | |
| | 75.98 | 76.02 | 75.98-P | ✓ | ✓ | | | | | | | | |
| | 76.12 | 76.22 | 76.12-U | | | ✓ | ✓ | ✓ | | | | | |
| | 76.23 | 76.33 | 76.23-T | ✓ | ✓ | ✓ | ✓ | | ✓ | | | | |
| | 76.35 | 76.43 | 76.35-P | ✓ | ✓ | | | | | | | | |
| | 86.74 | 86.85 | 86.74-U | | | ✓ | ✓ | ✓ | | | | | |
| | 86.85 | 86.96 | 86.85-T | ✓ | ✓ | ✓ | ✓ | | ✓ | | | | |
| | 86.96 | 87.06 | 86.96-U | | | ✓ | ✓ | ✓ | | | | | |
| | 87.07 | 87.18 | 87.07-T | ✓ | ✓ | ✓ | ✓ | ✓ | | | | | |
| | 93.92 | 94.02 | 93.92-U | | | ✓ | ✓ | ✓ | | | | | |
| | 94.03 | 94.07 | 94.03-P | ✓ | ✓ | | | | | | | | |
| | 94.07 | 94.15 | 94.07-P | ✓ | ✓ | | | | | | | | |
| | 99.01 | 99.12 | 99.01-P | ✓ | ✓ | | | | | | | | |
| | 99.17 | 99.28 | 99.17-U | | | ✓ | ✓ | ✓ | | | | | |
| | 99.28 | 99.39 | 99.28-U | | | ✓ | ✓ | ✓ | | | | | |
| | 109.01 | 109.12 | 109.01-U | | | ✓ | ✓ | ✓ | | | | | |
| | 109.12 | 109.23 | 109.12-T | ✓ | ✓ | ✓ | ✓ | | ✓ | | ✓ | | |
| | 109.23 | 109.33 | 109.23-T | ✓ | ✓ | ✓ | ✓ | | ✓ | | ✓ | | |

## 3.1 Physical, mechanical, and hydraulic properties

CanmetMINING's (CMIN) laboratory testing program included:

- sample preparation,
- measurement of physical properties (ultrasonic Vp and Vs, density, saturation porosity) and calculation of dynamic elastic constants (Poisson's ratio, Young's and shear moduli),
- determination of mechanical properties by UCS, TCS, and BTS testing, and
- estimation of intact rock permeability using constant head permeability testing.

Results are presented in Appendix A in spreadsheet and PDF formats.

### Sample preparation

Twelve core segments ranging in length from 0.1m to 0.8m were selected by the GSC and delivered to the CMIN laboratory. Segments were sub-sampled for each test to provide a vertical distribution of the key rock properties. Samples were prepared in accordance with internal Standard Operating Procedure (SOP) T-2121 and ASTM D4543-19. Fresh water was used for cutting and end preparation. Preparation of weathered Precambrian core samples was challenging due to the friability of the core and in some cases, hydrostone was required to repair the core ends to ensure test samples met surface flatness and parallelism tolerances. Each cylindrical core sample was assessed to ensure the dimensions and tolerances for end flatness and parallelism met internal and ASTM Standards. Photographs of representative samples, following preparation, are presented in Figure 9.


Figure 9. Representative prepared core samples. Left: BC81-2-4T (sandstone, 29.23 m); Centre: BC81-2-66.71-U (weathered granitic gneiss with hydrostone filling on the lower end, 66.71 m); Right: BC81-2-76.23-T (granitic gneiss with chlorite alteration, 76.23 m)

### Ultrasonic velocities

Ultrasonic pulse velocities (P- and S-wave) were measured on prepared core samples following ASTM D2845-08. It should be noted that this ASTM has been withdrawn without a replacement; however, this method is still considered valid for measurement of pulse velocities and calculation of the dynamic elastic constants. Tests were conducted at frequencies of 50KHz (P-wave) and 250KHz (S-wave) on dry, unconfined samples. Velocities are summarized in Table A.1 and Attachment A.

### Bulk density (dry/wet) and porosity

Core segments were weighed to determine their initial (as-received) density, and then oven dried at 110ºC (± 5ºC) until a constant mass was achieved to determine dry density. Following drying, samples were saturated by immersion in distilled water. The mass was recorded daily until a constant mass was achieved (less than 0.1% change relative to initial mass) to calculate final wet bulk density.

Porosity (n), the ratio of the volume of voids ($V_V$) to the total volume of the sample ($V_T$), was calculated based on the mass of the fluid ($m_F$) absorbed by the sample and the measured volume of the total sample:

$$n = V_V/V_T = (m_F/\rho_F)\, V_T \qquad [1]$$

where $\rho_F$ is fluid density (1g/cm$^3$). This methodology measures connected (effective) porosity, as isolated pores are assumed to be unaffected by the drying and saturation process. Densities and porosities are summarized in Table A.1 and Attachment A.

Saturated samples cut for the BTS testing were then transferred to CanmetENERGY labs for NMR testing prior to strength testing (see Section 3.2).

### Compression strength testing (UCS, TCS)

A total of 15 uniaxial (unconfined) compression strength tests (UCS) and eight triaxial (confined) compression strength tests (TCS) were conducted on rock core samples to determine strength and elastic properties (Young's modulus and Poisson's ratio). Samples were placed in heat shrink tubing and instrumented with mechanical gauges which consisted of three linear variable displacement transducers (LVDTs) to measure axial displacement and an MTS chain extensometer to measure radial displacement. Tests were conducted in accordance with internal standard operating procedures (SOP-T 2122) and standard test methods, specifically, ASTM D7012-14. Testing was completed using the servo-controlled MTS 815 loading frame (Figure 10) at a constant axial displacement rate of 0.0007mm/s. Samples were tested under dry conditions.

Compression strength test results are summarized in Table A.2. Stress-strain plots are included with detailed compression test data in Attachment B. Photographs of specimens, before and after failure, are included in Attachment C.

### Splitting tensile strength testing

Splitting tensile strength tests, also referred to as the Brazilian tensile strength (BTS) test, or indirect tensile strength test, were conducted on 26 specimens in accordance with internal standard procedures (SOP-T 2104) and standard test method ASTM D3967-16. Samples were tested using the MTS 815 loading frame at a constant load rate of 0.05kN/s.

Brazilian tensile strength test results are summarized in Table A.3, and photographs of failed specimens are included in Attachment D.


Figure 10. Strength and permeability testing were carried out using the servo-controlled MTS Rock Mechanics Testing System, Model 815. Photograph by S.Gaines. NRCan photo 2021-136.

## Permeability and hydraulic conductivity

Matrix permeability is an essential physical property of bedrock aquifers, defined by both the intrinsic or specific permeability (K) and the hydraulic conductivity (k). Intrinsic permeability is expressed in dimensions of a surface area and depends only on the properties of the medium (e.g. size of the pores or fractures, and the degree to which they are interconnected). Hydraulic conductivity is expressed in units of velocity and is a measure of the ease with which a fluid flows through a medium and therefore also depends on the properties of the fluid. These properties are linked by the equation:

$$k = K \rho_F (g/\mu_F) \quad [2]$$

where $\rho_F$ is the density of the fluid (kg/m$^3$), g is gravitational acceleration (in m/s$^2$), and $\mu$ is the dynamic viscosity of the fluid (kg/m s).

Hydraulic conductivity is calculated using Darcy's Law, which states that the volumetric flow rate (Q) through a porous medium over a time (t) is proportional to the flow area (A), the hydraulic conductivity (K), and the differential hydraulic head between two points ($\Delta$H) of separation L:

$$k = (Q * L) / (\Delta H * A * t) \quad [3]$$

$\Delta$H can also be defined as:

$$\Delta P / (\rho_F * g) \quad [4]$$

where P is the pressure measured at each end of the specimen. Intrinsic permeability (K) is calculated using the expression:

$$K = (k * \mu_F) / (\rho_F * g) \quad [5]$$

Constant head axial permeability tests were completed on three representative core specimens for the upper sandy dolostone and sandstone units to estimate the intact rock permeability (Figure 11). Axial permeability tests were conducted by inducing a hydraulic pressure gradient across a length, L, of a cylindrical rock specimen and measuring flow/discharge, Q, during the test. Core was encased in a thin layer of heat shrink tubing and subjected to confinement, $S_3$, higher than the maximum applied water pressure to prevent leakage outside of the rock specimen along the platen interface, or between the core and the heat shrink tubing. Constant pressure, $P_1$, was applied to the bottom of the core. No hydraulic pressure was applied to the top of the core specimens, creating a zero pressure/discharge boundary. Flow through the samples is achieved using specially designed grooved platens that allow water to enter/exit the bottom and top of the core, respectively.

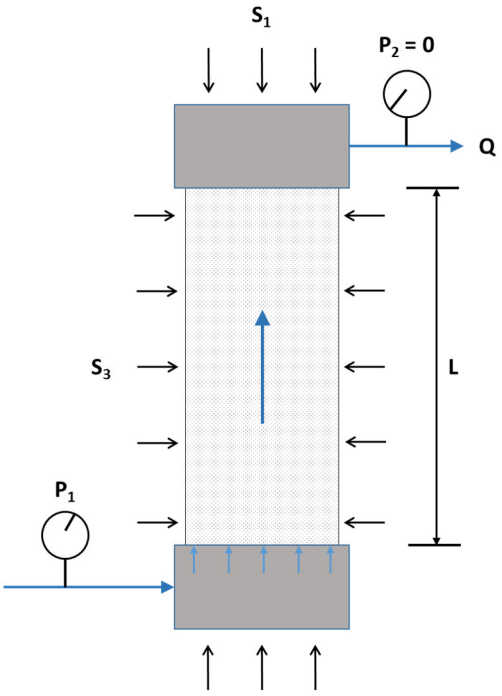


Figure 11. Schematic representation of the rock core constant head permeability test setup.

For this suite of tests, a confinement of 5 MPa and axial stress of approximately 10 MPa was applied to each saturated specimen prior to initiating a hydraulic gradient across the sample. Tests were completed using pressure control, with constant monitoring and servo-controlled feedback between the injection pressure ($P_1$) and fluid injection rate. Pressure and flow were monitored in real-time during testing by the test operator. Each step/stage was continued until a measurable fluid injection volume (> 1cm$^3$) was observed, or for a minimum of 1000s (~15min) following pressure stabilization. Where minimal fluid injection was observed, the time for each pressure step was extended to approximately 50-60 minutes.

Results of the axial permeability tests are summarized in Table A.4 and complete permeability test data are provided in Attachment E.

## 3.2 Nuclear magnetic resonance measurements

Nuclear magnetic resonance (NMR) measurements provide direct quantification of total water content, and estimations of pore size distributions and hydraulic conductivity (K) in geological materials. CanmetENERGY-Ottawa conducted NMR laboratory measurements on 11 saturated core samples (35mm in length, 47mm diameter) in the sedimentary bedrock using a low field Oxford Instruments 12MHz GeoSpec system. Five of these samples were also tested by H2 labs in Fredericton, NB, using an Oxford Instruments 2.36MHz GeoSpec-2 system. The data were collected as part of a study examining new slim-hole NMR logging tools which use lower frequencies (250 to 630kHz) and average over a larger vertical interval (0.15 to 0.50m) than the core samples (Pehme et al., 2021).

NMR systems use strong magnets to polarize the hydrogen found in a rock's pore fluids, and then apply a series of radio-frequency pulses to induce a spin-echo decay signal between each pulse (Dunn et al., 2002). The recorded spin-echoes between each pulse have diminishing amplitudes which are fit with a multi-exponential curve representing a relaxation time, called the $T_2$ curve. An inversion of the $T_2$ curve provides a $T_2$ amplitude distribution. The shape of the distribution contains information on the porous media and its pore fluids, and the area under the curve is proportional to the total water content of the sample. In a calibrated system, a linear relationship is established between signal amplitude and water content. Table 4 compares the results of the various porosity measurements (saturation and NMR) within the same samples.

Table 4. Comparison of saturated and NMR porosity measurements from three different labs (yellow highlight). Samples were 35mm in length and 47mm in diameter. Depths reported in meters below ground surface.

| Sample Name | Core Mid-point Depth (m) | Wireline Depth (m) | CANMET MINING Results | | CANMET ENERGY Results | | H2 Laboratories Results | | | |
|---|---|---|---|---|---|---|---|---|---|---|
| | | | Core Vol ($cm^3$) | Sat Por (%) | NMR Ave Water Content (mL) | NMR Por (%) | Water Mass (g) | Sat Por (%) | NMR Water Vol (mL) | NMR Por (%) |
| BC81-2-1B | 17.80 | 17.38 | 62.4 | 3.12 | 2.14 | 3.43 | 2.81 | 4.49 | 2.79 | 4.4 |
| BC81-2-2B | 29.83 | 29.42 | 61.59 | 12.42 | 7.63 | 12.38 | 8.03 | 13.05 | 7.90 | 12.6 |
| BC81-2-3B | 29.88 | 29.77 | 61.74 | 8.08 | 5.25 | 8.50 | | | | |
| BC81-2-4B | 34.67 | 34.26 | 61.77 | 1.02 | 0.89 | 1.45 | | | | |
| BC81-2-5B | 34.72 | 34.31 | 61.73 | 2.41 | 1.89 | 3.06 | 1.68 | 2.71 | 2.07 | 3.3 |
| BC81-2-6B | 34.76 | 34.35 | 61.27 | 4.55 | 2.82 | 4.60 | | | | |
| BC81-2-7B | 47.56 | 47.25 | 58.73 | 1.87 | 1.48 | 2.52 | 1.40 | 2.38 | 1.43 | 2.4 |
| BC81-2-8B | 59.23 | 59.04 | 62.28 | 8.85 | 5.63 | 9.04 | | | | |
| BC81-2-9B | 59.28 | 59.10 | 62.04 | 8.40 | 5.45 | 8.78 | | | | |
| BC81-2-10B | 59.92 | 59.74 | 61.91 | 9.35 | 5.70 | 9.21 | 6.04 | 9.80 | 6.02 | 9.7 |
| BC81-2-11B | 59.96 | 59.78 | 61.72 | 8.86 | 5.80 | 9.40 | | | | |

## 3.3 Complex resistivity measurements

In winter 2019/20, TechnoImaging LLC of Salt Lake City, Utah, conducted complex resistivity (CR) measurements as a function of frequency (0.01 to 1000Hz) on six core samples in the sandstone bedrock (TechnoImaging, 2021). During the testing, each of the samples was saturated in a vacuum system with a solution of increasing conductivity (5mS/m, 12mS/m, 20mS/m). The measured data were analysed using the generalized effective medium theory of the induced polarization effect (GEMTIP) (Zhdanov, 2008), and results showed that the sandstone exhibited distinct IP responses for the different saturating solutions.

Samples were selected in intervals displaying a range of properties. Samples 2B and 8B had elevated porosities (12.4% and 8.8% respectively), while samples 1B, 4B, and 7B had relatively lower porosities (3.1%, 1.0%, and 1.9% respectively). Sample 1R was chosen in a finer-grained interval that appeared to have a higher clay content based on a relatively elevated gamma log response. CR data (ρ) were analysed using the GEMTIP theory to model IP parameters of the rock samples, including chargeability (P), the time constant (τ), and the decay coefficient (C). Results of the measurements are provided in Table 5.

Table 5. Results of the complex resistivity measurements and GEMTIP IP parameter modeling using sandstone samples saturated with solutions of increasing conductivity. Depths reported in meters below ground surface.

| | **Sample Name** | **1B** | **2B** | **4B** | **1R** | **7B** | **8B** |
|---|---|---|---|---|---|---|---|
| | Porosity (%) | 3.12 | 12.42 | 1.02 | N/A | 1.87 | 8.85 |
| | Core Mid-point depth [m] | 17.80 | 29.83 | 34.67 | 37.44 | 47.56 | 59.23 |
| | Wireline Depth [m] | 17.38 | 29.42 | 34.26 | 37.06 | 47.24 | 59.04 |
| 5 mS/m solution | $\rho_{DC}$ [Ohm-m] | 725 | 445 | 1350 | 550 | 1300 | 430 |
| | P [%] | 3.5 | 31.5 | 0.575 | 2.25 | 10.75 | 15.75 |
| | τ [seconds] | 0.015 | 0.95 | 0.05 | 0.065 | 0.0975 | 0.575 |
| | C | 0.575 | 0.3 | 0.675 | 0.45 | 0.4 | 0.2025 |
| 12 mS/m solution | $\rho_{DC}$ [Ohm-m] | 720 | 330 | 1340 | 310 | 820 | 360 |
| | P [%] | 23.75 | 32.25 | 14 | 13.25 | 4.75 | 23 |
| | τ [seconds] | 0.25 | 0.825 | 0.095 | 0.75 | 0.145 | 0.65 |
| | C | 0.325 | 0.225 | 0.03 | 0.275 | 0.5 | 0.3 |
| 20 mS/m solution | $\rho_{DC}$ [Ohm-m] | 645 | 330 | 1250 | 295 | 720 | 335 |
| | P [%] | 34.5 | 16 | 11 | 22.5 | 17.25 | 22.25 |
| | τ [seconds] | 0.3 | 0.95 | 0.03 | 0.45 | 0.5 | 0.95 |
| | C | 0.225 | 0.35 | 0.425 | 0.25 | 0.325 | 0.3 |

The laboratory tests were carried out using saturating solutions with lower conductivities (5 – 20mS/m or 50 – 200µS/cm) than groundwater conductivities (300 - 650 µS/cm) which vary downhole depending on the depth and the season of measurement. As a result, the values using the 20mS/m solution will provide the closest guide to downhole IP measurements, but the calculated values should be adjusted to the actual conductivity of the fluids as measured at the time of logging. The key finding of this study is that the IP responses were distinct across all the sandstone samples, influenced by the porosity, matrix mineralogy, and importantly, by the conductivity of the saturating solutions.

# 4.0 Geophysical log data sets

## 4.1 Logging system and instruments

Following the casing repairs in 2019, a new suite of borehole geophysical logs was collected in BC81-2 to complement the existing data set compiled by Bernius (1996). Logs were acquired with a Matrix Data Logger acquisition system paired with a 4MXB winch (with 300m of 3/16" single conductor wireline), manufactured by Mount Sopris Instruments Ltd. During the logging, tool 'zero' was aligned with the top of the probe at the top of the surface casing, with a return-to-zero always completed at logging speed to assess any depth discrepancies. **Note that geophysical logs presented in Appendix B have depths relative to top of casing.** The log suite and acquisition parameters are listed in Table 6, with data sets provided in Appendix B. Log data were imported into WellCAD v5.4 (build 1415) processing software for analyses and display. Readers without WellCAD can download the WellCAD Reader at no cost to view the file (https://www.alt.lu/download/).

Table 6. Log suite acquired in BC81-2 in 2019 with acquisition details.

| Logging Tool | Logging Unit | Model | Direction | Average Logging Speed (m/min) | Vertical Sampling rate |
|---|---|---|---|---|---|
| Optical Televiewer | RGB colour intensity | ALT QL40-OBI40 | Up | 0.7 | 0.125 cm |
| Acoustic Televiewer | Traveltime, amplitude | ALT QL40-ABI40 | Up | 0.6 | 0.125 cm |
| Total Gamma | Counts per second (cps) | MS 2SNA | Up | 0.55 | 1 cm |
| Full Waveform Sonic | Traveltime, amplitude | ALT QL40-FWS 1TX-4RX | Up | 2 | 5 cm |
| Fluid Temperature | °C | MS QL-FTC probe body + GSC thermistor | Down | 1 | 1 cm |
| | °C | RBRsolo$^3$T | Down | 1 | 2 Hz |
| Fluid Conductivity | µS/cm | MS QL-FTC | Down | 1 | 1 cm |
| Heat Pulse Flow Meter | L/min | MS HFP-2293 | N/A | Stationary | Various |

## 4.2 Wireline depth calibrations

Depth has been described as the most fundamental logging parameter as it ties together all subsurface measurements. The quality of depth measurement for wireline logs has been studied by the petroleum industry for decades, examining issues including cable stretch, encoder wheel accuracy, temperature, buoyancy, pressure, and friction (e.g. Bolt, 2016). In calibration boreholes, the issue of depth accuracy for both wireline logs and core is particularly important. Prior to undertaking logging in BC81-2, a series of lab and field tests were carried out to evaluate the accuracy of the depth counting system on the GSC's logging winch over a 100-m interval.

Lab tests

The depth counting system used a single measuring wheel (1/3m circumference) with an optical encoder mounted on the winch. A new measuring wheel was installed prior to the logging to eliminate any systematic depth errors that could be introduced by grooves or wear in an older wheel. The accuracy of the encoder, which counts 800 pulses per wheel revolution, was tested over 72,000 pulses (equivalent to a 300m length) in both down (forward) and up (reverse) directions. The mechanism that applies pressure between the counter wheel and the cable was disabled to allow the wheel to rotate freely. During the test the winch motor was left to run at a low speed (barely moving) in an attempt to simulate electrical noise from the motor. A mark was made on the wheel and on an appropriate spot on the frame to allow for accurate counting. A push button counter was used to count the revolutions manually. The wheel was rotated 100 times and the pulse count recorded; this was done to a total count of 900 revolutions. At the 900$^{th}$ count, the wheel was rotated in the opposite direction 900 times back to 0. Results indicated the encoder read the exact number of counts (up and down) and was working well within specification for the maximum depth logged at Bells Corners (Table 7).

Table 7. Results of encoder pulse tests in the lab, indicating accuracy of counts over measuring wheel revolutions equivalent to 300m of wireline.

| Down Direction (+) | | | Up Direction (-) | | |
|---|---|---|---|---|---|
| Rev (#) | Pulse Count | Distance (m) | Rev (#) | Pulse Count | Distance (m) |
| 0 | 0.0 | 0 | 0 | -72000.1 | -300.000 |
| 100 | 8000.0 | 33.333 | -100 | -64000.1 | -266.667 |
| 200 | 16000.1 | 67.667 | -200 | -56000.1 | -233.334 |
| 300 | 24000.1 | 100.00 | -300 | -48000.1 | -200.000 |
| 400 | 32000.1 | 133.33 | -400 | -40000.1 | -166.667 |
| 500 | 40000.0 | 167.67 | -500 | -32000.1 | -133.334 |
| 600 | 48000.0 | 200.00 | -600 | -24000.1 | -100.000 |
| 700 | 56000.1 | 233.33 | -700 | -16000.1 | -66.667 |
| 800 | 64000.0 | 266.67 | -800 | -8000 | -33.333 |
| 900 | 72000.1 | 300.00 | -900 | 0 | 0 |

Field tests

In theory, three revolutions of the counting wheel (2400 encoder pulses) would be equivalent to 1.00m of wireline. To test this in practice, depth calibrations were performed for each logging tool over 100m of wireline. As each tool has a different weight, buoyancy in water, and friction with the wall (if it uses bowspring arms for (de)centralization), tests were performed on each tool suspended downhole to re-create real logging conditions. Depth calibrations were run in both up and down directions to investigate any differences from factors like stretch or drag. Air temperature and water temperature/levels were considered. Initial tests were run in July when air temperatures ranged from 20.5 to 29°C (and water temperatures ranged from 7.9 – 8.7°C). The tests were run again in October when air (8.2 – 10.4°C) and water (8.3 – 8.9°C) temperatures were in close range to reduce any effects from system temperature fluctuation.

A measuring tape was fixed to the cable at a 0.00m scribe mark (but placed under no tension from the wireline) and tape+wireline were lowered together down to a depth of 100m. Scribe marks were written on the wireline every 10m for each tool. Each tool was run up and down the hole twice to record the number of encoder pulses in the up and down directions over 100m. The number of pulses were averaged to determine an encoder factor for each tool, and then run a third time using the factor to measure how close each run was to 100m. The encoder factors ranged from 2393 to 2397, producing measurable uncertainties of 1 to 3cm in 100m (Table 7). Differences in air temperature between July and October did not appear to have an impact on encoder factors.

This approach is only as accurate as the method used to independently measure 100 metres on the wireline. A heavy-duty NIST fibreglass tape was used for these studies and care was taken to avoid slippage or wrapping of the tape on the wireline, but some epistemic error will be present no matter what approach is used to measure 100 m. This empirical approach indicated there are some small differences in the encoder factors of the up and down runs, but didn't resolve the cause(s). This approach doesn't account for any non-systematic factors like cable slip, which still needs to be assessed for each logging run using a "return-to-zero" depth measurement verification. As the factors in Table 8 were uniquely determined specifically for this encoder/logging system in these boreholes, they are not for application to other logging systems.

Table 8. Encoder factors used in this study to calibrate wireline depths over 100m in BC81-2.

| Tool | Average down factor | 100 m test using factor | Average up factor | 100 m test using factor |
|---|---|---|---|---|
| Optical televiewer | 2393 (July) | 100.02 | 2396 (July)<br>2396 (Oct) | 100.01<br>100.02 |
| Acoustic televiewer | 2394 (July)<br>2394 (Oct) | 99.99<br>- | 2396 (July)<br>2397 (Oct) | 100.01<br>100.01 |
| Spectral Gamma | 2394 (July) | 100.01 | 2396 (July) | 99.99 |
| Full Waveform Sonic | 2397 (July) | 100.00 | 2397 (July) | 100.03 |
| Magnetic Susc/Conductivity | 2393 (July)<br>2394 (Oct) | 99.99<br>- | 2396 (July)<br>2396 (Oct) | 100.02<br>100.02 |
| Fluid temperature/conductivity | 2396 (July)<br>2396 (Oct) | 100.03<br>100.02 | -<br>- | -<br>- |

## 4.3 Relationship between wireline depths and core depths

While examining the core alongside the new geophysical logs, discrepancies were noted between the two sets of depths. For these comparisons, geophysical log depths were adjusted for casing stick-up so both core and logs could be examined with the same depth reference of metres below ground surface. High resolution downhole optical televiewer (OTV) images were used to relate calibrated wireline depths to core depths. At the Paleozoic-Precambrian contact, the depths were the same, but the discrepancy increased in step-wise increments to -58cm at the top of rock, and to +21cm at the base of the borehole. It seems that the original core depths were calibrated at the contact using the original wireline logs, and measured upward and downward to the top and bottom of the borehole. Loss of core in fractured or brecciated zones appears to account for much of the discrepancy (Figure 12).

Prominent geological features (e.g. veins, joints, fractures, bedding, etc.) that were readily identifiable on both the core and the OTV log were used to relate core depths to calibrated wireline depths. In total 55 features were observed. An interpolated depth correction was created at 10cm intervals to align the core depths with responses recorded by the wireline tools in meters below ground surface. In this report, all core measurements are reported in core depths to remain consistent, but also provided in wireline depths using the correction table provided in Appendix B.

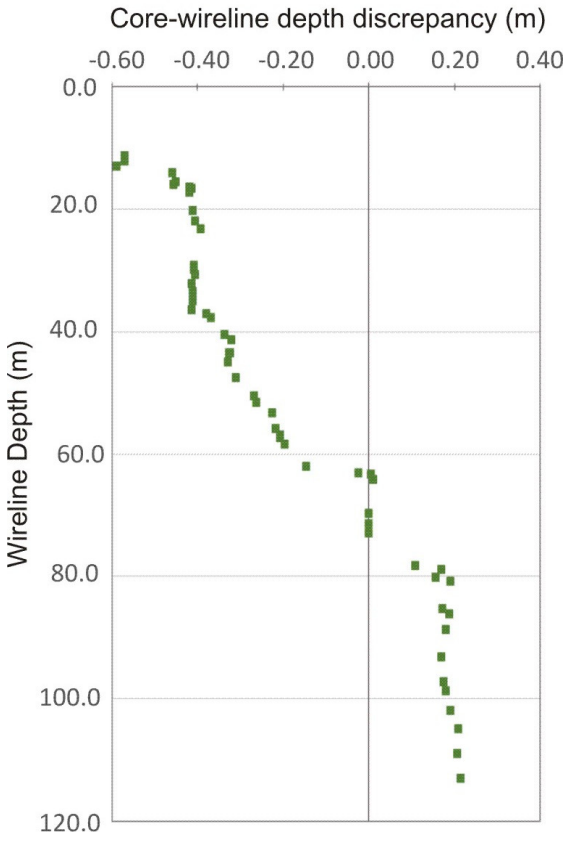


Figure 12. Discrepancies measured between calibrated wireline depths and core depths (both in meters below ground surface) using 55 recognizable geological features in the core and the optical televiewer log.

## 4.4 Downhole log summary

A brief overview of the new logs acquired in 2019 is presented below and summarized in the log suite shown on Figure 13. Digital data (WellCAD, LAS, Excel files) can be found in Appendix B.

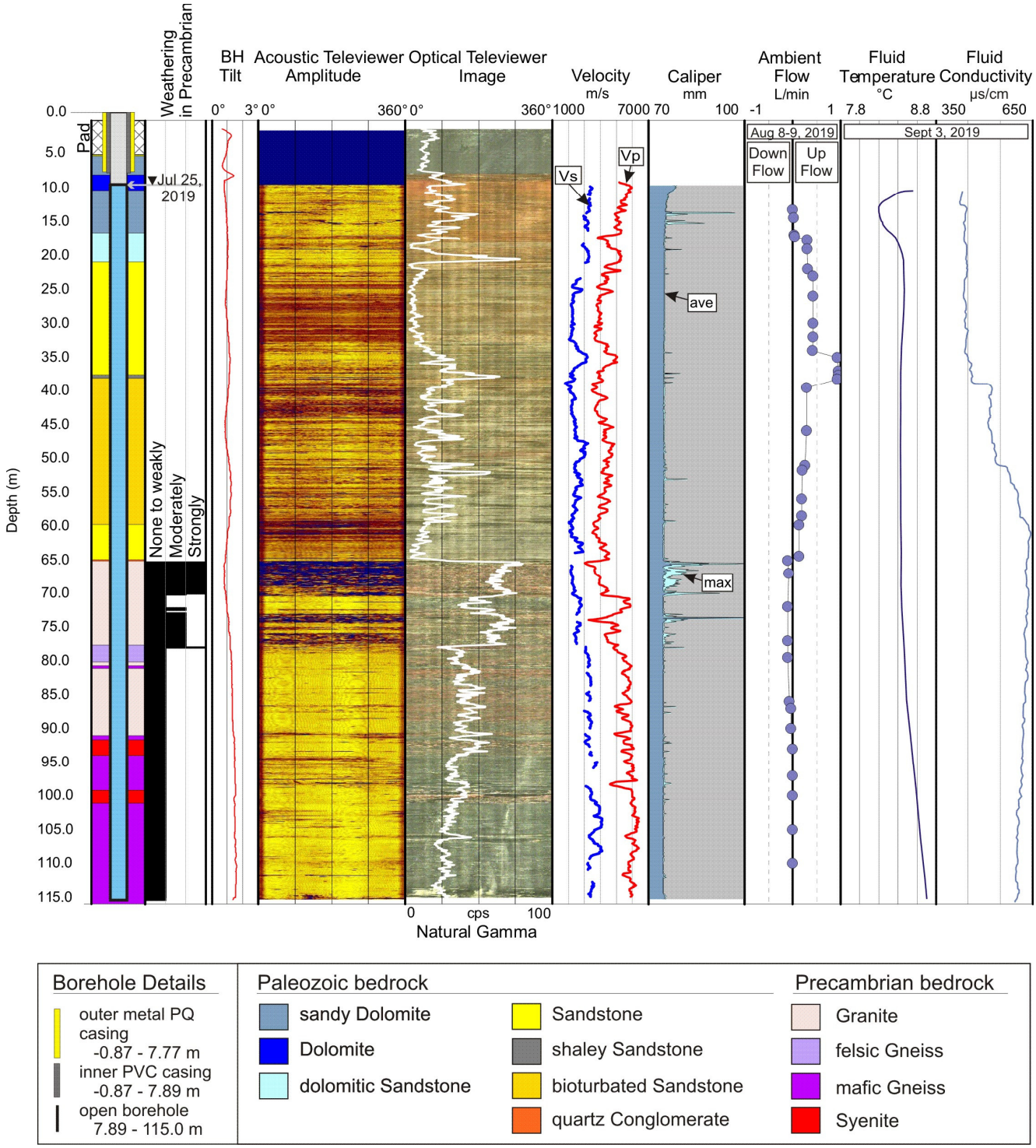


Figure 13. Summary plot of new logs acquired in BC81-2 in 2019. Depths are relative to top of casing.

## Borehole imaging

Borehole televiewers provide a method of imaging the borehole wall in high resolution using either digital colour scans (optical televiewer, OTV), or ultrasonic pulses (acoustic televiewer, ATV). The tools require centralization in the borehole, achieved using two sets of bowspring arm centralizers, made of non-magnetic material.

Both televiewers were equipped with an APS544 orientation sensor, containing a 3-axis magnetometer and 3 accelerometers. For each scan of the borehole wall, the sensor resolves magnetic north and the tilt of the tool with an accuracy of 1° (azimuth) and 0.5° (tilt). This allows for the orientation of images to magnetic north (in vertical or angled holes) or borehole high-side (in angled holes) to maintain a common reference direction for structural interpretation. The tilt log provides the inclination of the hole from vertical, and is also used to correct the dip/dip direction of interpreted structures from apparent to true dips. In BC81-2, the borehole tilt increases slightly from 0.7° in the near surface to approximately 1.6° at the base of the borehole. In rock of elevated magnetic susceptibility, such as much of the Precambrian bedrock at the Bells Corners site, the magnetometer cannot be used to reliably orient the image. For this reason, images are provided both unoriented and oriented to magnetic north in the WellCAD file.

### *Acoustic televiewer*

The ATV transmits pulses from a fixed transducer through a rotating focusing mirror, recording the amplitude and traveltime of the signal reflected by the borehole wall. The ATV records the entire reflected wavetrain and must be run in fluid for pulse transmission. Processing algorithms allow the software in real time to determine the first reflection from the tool's acoustic window, followed by the reflection from the bedrock wall, and other subsequent reflections. The logging software records both the amplitude and the traveltime of the reflection from the borehole wall. Line scans of the borehole were collected in 1.25 mm increments at a maximum resolution of 288 pixels/revolution.

The amplitude image indicates a number of discontinuities (fractures) extending into the borehole wall, as well as partial fractures and closed, hairline features (e.g. joints). Finer detail such as changes in reflectivity from bed to bed and within bioturbated zones could be identified. The 360° traveltime data were used to calculate an acoustic caliper log assuming a fluid velocity of 1480m/s. The software calculates a minimum, maximum, and average borehole diameter, the later of which was verified against the driller-reported diameter of the borehole of 76mm. The mean of the average borehole diameter was 76.12 ± 1.18mm (1 standard deviation).

### *Optical televiewer*

The OTV used a high sensitivity charge-coupled device (CCD) digital camera with Pentax optics for full colour imaging of the borehole wall surface in air or clear water. The stationary camera is located above a conical mirror that spins during logging, capturing the reflection of the borehole wall. Light for the recording is provided by a ring of LED lights above the optical head. Line scans of the borehole wall were collected in 1.25mm increments at a resolution of 1.25 pixels/degree.

The OTV provides high-resolution colour images of lithological features such as bedding, cross-bedding, bioturbation, and banding, and detail on *in situ* structural features such as fractures, joints, and some evidence of alteration. While analyses of structural orientations did not form part of this report, the OTV data was used extensively for the core depth calibrations, and to identify the presence, size, and appearance of fractures in the borehole wall to support fluid log interpretation.

## Gamma methods

Gamma logs measure naturally occurring radioactivity by converting gamma rays emitted from the formation into electronic pulses using a scintillator crystal in the tool. The most common natural radionuclides in rock and sediment are potassium (K), uranium (U), and thorium (Th). Radioactive decay is statistical in nature and photon emission follows a Poisson's distribution. The standard deviation of the count number will be its square root, therefore, the relative accuracy of the measurement is greater at higher count rates, requiring slow logging speeds to achieve longer sampling periods (≤1m/min).

The gamma log has the same trends as the logs acquired in the 1990's. Count numbers between the new and the older tools scale differently due to differences in tool design, but they respond to the same lithological changes described by Bernius (1996). The new total count gamma log is included in this data release to provide a digital gamma log in counts per second (not calibrated API units) collected at a known, slow (0.55m/min) logging rate.

## Sonic methods

Full waveform sonic (FWS) tools record amplitudes and traveltimes of high frequency pulses used to interpret compressional (P) and shear (S) wave slowness (inverse of velocity) along the borehole wall. A 15kHz transmitter at the base of a centralized sonic probe radially emitted pulses into the fluid-filled portion of the borehole. P-wave energy refracted at the borehole wall as compressional and shear head waves, and reflected as numerous modes, was recorded over a 3ms record length by four receivers located 0.6m, 0.8m, 1.0m, and 1.2m above the transmitter.

Data were processed using a velocity analysis technique called semblance processing that looks for similarities in waveforms across all four receivers. Paillet and Cheng (1991) provide a description of the semblance cross-correlation technique developed for sonic data in an open borehole. The semblance algorithm starts with an assumed slowness and computes a coherence value for the four receivers, then moves on to the next record. A plot of coherence maxima versus record depth was generated and analyzed for the refracted P- and S- head wave slowness (Figure 14). A first analysis was carried out without filtering the waveforms, producing clear P-wave and generally clear S-wave coherence maxima. A bandpass filter with corner frequencies of 0-5-25-32kHz was also used to remove low frequency noise and sharpen the S-wave coherence. A check on the P- and S-wave velocity analyses was performed by calculating P- and S-wave velocities from transit times of picked P- and S-wave arrivals from receivers 1 and 2. The arrival times were filtered with a 3 point weighted average filter and the velocities were computed by dividing the difference between the transit times into the distance between them (0.2m). The P- and S-wave velocities are shown superimposed on Figure 14. Although the semblance approach smooths out peaks and troughs that are present when using an individual trace picking approach, the two approaches were generally in close agreement.

In some intervals, however, the S-wave coherence was weak. Examination of the waveforms in these intervals indicated a loss of S-wave signal amplitude and coherence (Figure 15). This created abrupt increases in the S-wave slowness maxima that weren't always in agreement with the trends of the P-wave slowness or the average Vp/Vs ratios calculated from the core measurements. At these depths, the S-wave velocity is removed from the log until further testing can be carried out.

Over the borehole length, interpreted P-wave velocities range from 3000 to 6500m/s, and S-wave velocities from 1700 to 4100m/s. These ranges include intervals containing fractures and/or weathered zones in the borehole wall where signal coherence is often reduced; therefore analyses of velocity ranges

in particular rock types must be undertaken with reference to caliper and televiewer logs. Bedrock velocity analyses are a topic of ongoing study at the Facility.

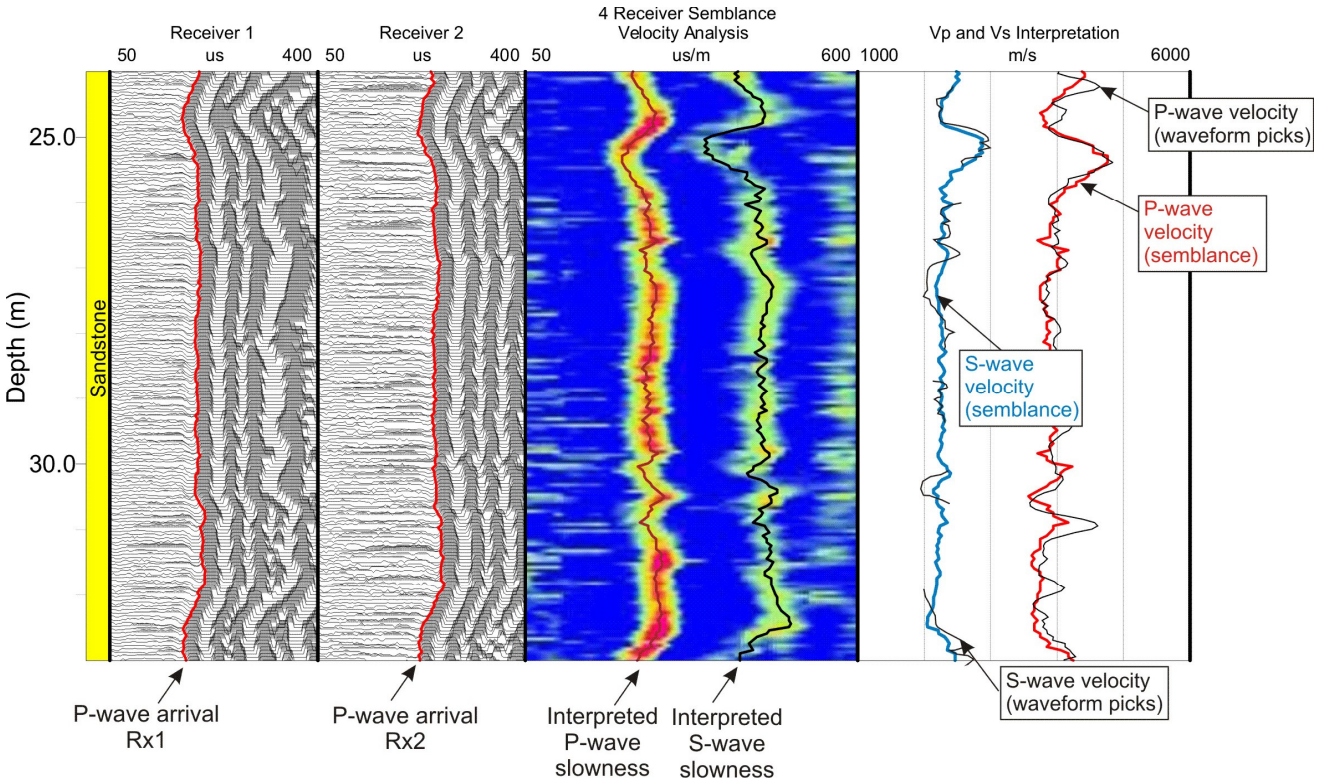


Figure 14. Velocity analyses from full waveform sonic data collected in BC81-2. First arrivals and later S-wave arrivals were picked from waveforms recorded by receivers 1 and 2 to compute P- and S-wave velocities. Coherence analysis from semblance processing allowed for an interpretation of P and S-wave slowness, from which P- and S-wave velocities were calculated. Velocity logs from both analysis approaches are overlaid for comparison.

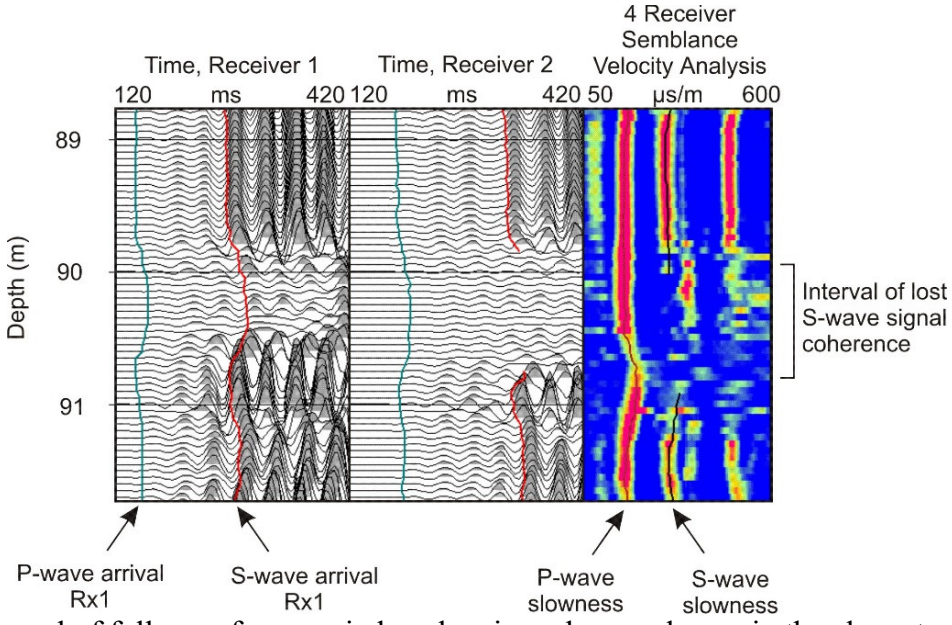


Figure 15. Interval of full waveform sonic log showing where a change in the character of the S-wave arrivals results in a loss of S-wave signal coherence in semblance processing.

## Fluid logging methods

### *Fluid temperature/conductivity*

Fluid logging tools record changes in fluid properties as they descend along the borehole. A dual fluid temperature/fluid conductivity probe was used for the logging with sensors mounted inside, or on the tip of, the nose cone. The temperature sensor supplied with the tool is a linear, fast-response semi-conductor located inside a stainless steel sealed tube (stinger) recessed 9.5cm inside the nose cone. Thermal grease is used to reduce thermal resistance between the sensor, the steel stinger, and the logging environment. The reported accuracy is <1% (resolution ±0.004°C) over a range of -20 to 80°C, but the sensor is detecting an averaged temperature due to its position within a steel chamber inside the nose of the tool.

To collect higher resolution temperature data with faster thermal response, the probe was adapted with the addition of an exposed thermistor at the tip of the nose cone, designed and mounted by the GSC. This approach resulted in several advantages:

- Thermistors are more sensitive than their integrated circuit temperature counterparts. The exposed thermistor bead has the lowest possible thermal resistance to the borehole fluid, increasing its overall accuracy and step response by removing the thermal resistance created by the stinger assembly; and
- The position of the bead at the tool tip
    - reduces the effect of the tool's thermal mass on the surrounding borehole fluid temperature; and
    - reduces the effects of turbulence in the water column (i.e. mixing of any temperature stratification inside the nose cone) as the tool descends.

There are risks to an exposed thermistor including damage from physical impacts and chemical corrosion. Fortunately, thermistors are generally inexpensive and the position of the thermistor on the outside of the tool makes it relatively easy to replace.

Fluid conductivity was measured using a seven electrode mirrored Wenner array located inside the nose cone of the tool. The response is manufacturer-calibrated within a range of 5 to 300,000µS/cm. Fluid conductivities were collected both uncorrected for temperature and corrected to 25°C (for comparison with a field calibration instrument), and are reported as-measured (i.e. uncorrected for temperature).

For quality control, instrument readings were compared to those of a calibrated Oakton hand-held fluid conductivity meter and a calibrated Thermoprobe TL1-R digital stem thermometer in groundwater samples brought to surface. Additionally, a high-resolution, stand-alone temperature logger (RBRsolo$^3$T, RBR Ltd.), manufacturer-calibrated to an accuracy of ±0.002°C, was temporarily affixed to the outside of the probe with the temperature sensor at the same position as the thermistor bead on the tool tip during the logging. These data were compared alongside the thermistor log, and data sets are provided in Appendix B.

To avoid disturbing the water column, the fluid logging tool was the first instrument run downhole at a logging speed of 1m/min. On September 3, 2019, the fluid temperature ranged between 8.19 and 8.70°C and the fluid conductivity ranged from 418 and 646µS/cm (Figure 13). To investigate the variability of fluid temperature with season, repeat runs were collected over the year and recorded only after the borehole had restabilized for 48 or more hours. In 2019, the high-resolution temperature logs indicate a repeatable response below approximately 27.5m ranging from approximately 8.45°C to 8.70°C near

the base of the hole. The logs above this depth indicate seasonal variability in fluid temperatures, as shown in Figure 8. Investigation of these variable temperature and conductivity log responses is a topic of ongoing research.

### *Heat pulse flow meter*

The heat pulse flow meter (HPFM) is based on a US Geological Survey design to measure low-velocity, vertical borehole flow (Hess, 1982, 1986). The flowmeter contains a heating grid with equidistant temperature sensors positioned a few centimetres above and below the grid. Rubber diverter petals centralize and seal the probe in the borehole, forcing the fluid to pass through a wire mesh over the heating grid and the sensors. When the tool is positioned for a series of readings, a heat pulse is triggered by the operator. The grid heats a lens of water that moves up or down with the flow of the borehole fluid past the sensor array. An amplifier detects the difference in temperature between the sensors, and converts the output to a frequency which is sent up the cable and recorded by the laptop. The software records the time elapsed between the heat pulse trigger and the measured peak temperature change, which is converted to flow using manufacturer calibration values. The tool is designed to detect flows ranging between 0.11 and 3.78L/min. Very small flows can be detected with extended time windows if the borehole fluid is given sufficient time to equilibrate around the tool, but this can be very time consuming.

The HPFM was the final tool run in the well after examination of televiewer and fluid logs. Target depths were selected above and below fractures to identify intervals where fluid was being transmitted into or out of the borehole. A total of 135 tests were conducted at 37 depth intervals over three days; results are provided in an Excel table in Appendix B. Fluid was found to be entering the borehole through a fracture at the base of the sandstone interval and flowing up from the fracture, and downward below it. Through the sandstone interval, up flows in August 2019 ranged between 0.13 and 0.96L/min. No flows were recorded above 13.25m (btoc). Down flows ranged between 0.03 and 0.1L/min, until no flow was detected below 93.0 m (btoc).

## 5.0 Site access

This report provides new core and downhole log data sets from borehole BC81-2 to support ongoing tool calibration, methods and instrument development, and research into regional geology and bedrock-groundwater interaction. The installation of atmospheric monitoring equipment in 2019 also provides new information to support shallow groundwater research in the Ottawa area. Cores continue to be available for viewing and testing, provided the data is shared with the GSC.

To discuss research opportunities or site access, please contact the GSC at:

< bellscornerscalibrationfacility@NRCan-RNCan.gc.ca>

## 6.0 Acknowledgments

The authors wish to thank: John Hogan for continued Facility support at the CANMET Complex, Marathon Underground for repair work on the deep boreholes, Michael Zhdanov and Doug Pitcher for coordinating and overseeing the resistivity testing on the cores, Barbara Dietiker for discussions on the bedrock velocity interpretations, Laura Olson for work on the wireline logs, Rick McNeil for core retrieval, Catherine Béland-Otis and Claire Milloy for discussions related to local bedrock and groundwater conditions, and Peeter Pehme for review of this report.

Funding was provided through the Geological Survey of Canada's Groundwater Geoscience, Public Safety Geoscience, and Environmental Geoscience Programs.

# 7.0 References


ASTM Standard D4543-19, 2019. Standard practices for preparing rock core as cylindrical test specimens and verifying conformance to dimensional and shape tolerances, ASTM International, West Conshohocken, PA.

ASTM Standard D2845-08, 2008. Standard test method for laboratory determination of pulse velocities and ultrasonic elastic constants of rock (withdrawn 2017), ASTM International, West Conshohocken, PA.

ASTM Standard D7012-14, 2014. Standard test methods for compressive strength and elastic moduli of intact rock core specimens under varying states of stress and temperatures, ASTM International, West Conshohocken, PA.

ASTM Standard D3967-16, 2016. Standard test method for splitting tensile strength of intact rock core specimens, ASTM International, West Conshohocken, PA.

Bernius, G.R., 1981. Boreholes near Ottawa for the development and testing of borehole logging equipment – a preliminary report; *in* Current Research, Part C, Geological Survey of Canada, Paper 81-1C, p. 51-53. https://doi.org/10.4095/116175

Bernius, G.R., 1996. Borehole geophysical logs from the GSC Borehole Geophysics Test Site at Bell's Corners, Nepean, Ontario. Geological Survey of Canada, Open File 3157, 38 p. https://doi.org/10.4095/207617

Bernstein, L., 1992. A revised lithostratigraphy of the Lower-Middle Ordovician Group, St Lawrence Lowlands, Quebec and Ontario; Canadian Journal of Earth Sciences, v. 29, p. 2677-2694.

Bolt, H., 2016. Wireline logging depth quality improvement: Methodology review and elastic stretch correction; Petrophysics, v. 57, p. 294-310.

Charbonneau, B.W., Jonasson, I.R., and Ford, K.L., 1975. Cu-U mineralization in the Mach Formation Paleozoic rocks of the Ottawa-St. Lawrence Lowlands; *in* Report of Activities, Part A, April to October 1974; Geological Survey of Canada, Paper no. 75-1A, p.229-233. https://doi.org/10.4095/247867

Chiarenzelli, J., Aspler, L.B., Donaldson, J.A., Rainbird, R., Mosher, D., Regan, S.P., Ibanez-Meija, M., and Franzi D.A., 2010. Detrital zircons of Cambro-Ordovician sandstone units in eastern Ontario and northern New York: Geological Society of America Abstracts with Programs, v. 42, no. 118.

Corriveau, L., Heaman, L.M., Marcantonio, F., and van Breemen, O., 1990. 1.1 Ga K-rich alkaline plutonism in the SW Grenville Province; Contributions to Mineralogy and Petrology, v. 105, p. 473-485. https://doi.org/10.1007/bf00286834

Davidson, A. 1998. An overview of the Grenville Province geology, Canadian Shield, Chapter 3, *in* Geology of the Precambrian Superior and Grenville Provinces and Precambrian Fossils in North America; by Lucas, S.B. and St-Onge, M.R.; Geological Survey of Canada, Geology of Canada, Series no. 7, p. 205-270 (also Geological Society of America, The Geology of North America,v. C-1). https://doi.org/10.4095/210103

Delcan, 1983. Stony Swamp Conservation Area Hydrogeological Study; Delcan Consulting Engineers and Planners, Report 041292A00.

Di Prisco, G., and Springer, J.S., 1991. The Precambrian-Paleozoic unconfiormity and related mineralization in southeastern Ontario; Ontario Geological Survey, Open File Report 5751, 122p. Retrieved June 23, 2021 from http://www.geologyontario.mndmf.gov.on.ca/mndmfiles/pub/data/imaging/OFR5751/OFR5751.pdf

Dix, G.R., Salad Hersi, O., and Nowlan, G.S., 2004. The Potsdam-Beekmantown Group boundary, Nepean Formation type section (Ottawa, Ontario): A cryptic sequence boundary, not a conformable transition; Canadian Journal of Earth Sciences, v. 41, p. 897-902.

Dunn, K.J., Bergman, D.J., and Latorraca, G.A., 2002. Nuclear Magnetic Resonance Petrophysical and Logging Applications. Oxford, United Kingdom, Elsevier Science, 293p.
Easton, R.M., 1992. The Grenville Province and Proterozoic history of central and southern Ontario; *in* Geology of Ontario, (ed.) P.C. Thurston, H.R. Williams, R.H. Sutcliffe, and G.M. Scott; Ontario Geological Survey, Special Volume 4, Part 2, p. 715-904.
Google, n.d. City of Ottawa. Retrieved June 9, 2021 from https://www.google.ca/maps/@45.3886681,-75.689456,11.75z
Hoekstra, H.R., and Fuchs, L.H., 1960. Economic Geology, v.55, p 1716 – 1738.
Hofmann, H.J., 1998. Synopsis of North American stratigraphic units with remains reported as pre-Cambrian, Figure 4-1 *in in* Geology of the Precambrian Superior and Grenville Provinces and Precambrian Fossils in North America; by Lucas, S.B. and St-Onge, M.R.; Geological Survey of Canada, Geology of Canada, Series no. 7, p. 205-270 (also Geological Society of America, The Geology of North America,v. C-1). https://doi.org/10.4095/210103
IAEA, 1976. Radiometric reporting methods and calibration in uranium exploration; International Atomic Energy Agency, Technical Report Series no. 174, 57 p.
Killeen, P.G., 1978. Gamma-ray spectrometric calibration facilities – a preliminary report; *in* Current Research, Part A, Geological Survey of Canada, Paper 78-1A, p. 243-247. https://doi.org/10.4095/119799
Killeen, P.G., and Conway, J.G., 1978. New facilities for calibrating gamma-ray spectrometric logging and surface exploration equipment; Canadian Institute of Mining and Metallurgical Bulletin, 793, p. 84-87.
Killeen, P.G., Bernius, G.R., Schock, L., and Mwenifumbo, C. J., 1984. New developments in the GSC borehole geophysics test area and calibration facilities; in Current Research, Part B, Geological Survey of Canada, Paper 84-1B, p. 373-374. https://doi.org/10.4095/119597
Killeen, P.G., 1986. A system of deep test holes and calibration facilities from developing and testing new borehole geophysical techniques; in Borehole Geophysics for Mining and Geotechnical Applications, e.d. P.G. Killeen, Geological Survey of Canada, Paper 85-27, p. 29-46. https://doi.org/10.4095/123596
Lowe, D.G., 2016. Sedimentology, stratigraphic evolution and provenance of the Cambrian-Early Ordovician Potsdam Group in the Ottawa Embayment and Quebec Basin. Ph.D. thesis, Department of Earth Sciences, University of Ottawa, Ontario.
Lowe, D.G., Arnott, R.W.C, Chiarenzelli, J.R., and Rainbird, R.H. 2018. Early Paleozoic rifting and reactivation of a passive-margin rift: Insights from detrital zircon provenance signatures of the Potsdam Group, Ottawa graben; GSA Bulletin, v.130, p.1377-1396
Mwenifumbo, C.J., Elliott, B.E., Hyatt, W.G., and Bernius, G.R., 2005. Bells Corners calibration facilities for downhole and surface geophysical equipment. Geological Survey of Canada, Open File 4838, 17 p. https://doi.org/10.4095/216755
Pehme, P., Crow, H.L., Parker, B., Russell, H.A.J., 2021. Evaluation of slim-hole NMR logging for hydrogeologic insights into dolostone and sandstone aquifers; Journal of Hydrogeology (*in press*).
Salad Hersi, O., Lavoie, D., and Nowlan, G.S., 2003. Reappraisal of the Beekmantown Group sedimentology Quebec: implications for understanding the depositional evolution of the Lower-Middle Ordovician Laurentian passive margin of eastern Canada; Canadian Journal of Earth Science, v. 40, p. 149-176.
Salad Hersi, O., and Dix, G.R., 2006. Precambrian fault systems as control on regional differences in relative sea level along the early Ordovician platform of eastern North America; Journal of Sedimentary Research, v. 76, p. 700-716.

Sanford, B.V., and Arnott, R.W.C., 2010. Stratigraphic and Structural Framework of the Potsdam Group in eastern Ontario, western Quebec and northern New York State; Geological Survey of Canada, Bulletin 597, Geological Survey of Canada, Ottawa, Ontario. https://doi.org/10.4095/247669

Schock, L.D., Killeen, P.G., Elliott, B.E., and Bernius, G.R., 1996. A review of Canadian calibration facilities for borehole geophysical measurement, *in* Borehole geophysics in mineral exploration: Short course manual, (ed.) P.G. Killeen, C.J. Mwenifumbo, B.E. Elliot, K.A. Pflug, L.D. Schock, and G.R. Bernius; Geological Survey of Canada, Open File 3247, p. 40-51 (also Proceedings of the 4th international symposium on borehole geophysics for mineral and geotechnical logging, August 18-22, 1991, Toronto, Ontario, p. 191-202). https://doi.org/10.4095/207612

TechnoImaging, 2021. Complex resistivity (CR) measurements of the sandstone and shale rock samples from the Bells Corners GSC borehole geophysics test site, Canada; Internal report, February 2021.

Wynne-Edwards, H.R., 1972. The Grenville Province. Geological Association of Canada Special Paper 11: 163-182

Zhdanov, M. 2008. Generalized effective-medium theory of induced polarization. Geophysics 73: F197-F211. https://doi.10.1190/1.2973462